The Astrophysical Journal, 692:1447–1463, 2009 February 20 doi:10.1088/0004-637X/692/2/1447

ΛCDM SATELLITES AND H I COMPANIONS—THE ARECIBO ALFA SURVEY OF NGC 2903

Judith A. Irwin[1], G. Lyle Hoffman[2], Kristine Spekkens[3], Martha P. Haynes[4,14], Riccardo Giovanelli[4,14], Suzanne M. Linder[5], Barbara Catinella[6,15], Emmanuel Momjian[7,16], Bärbel S. Koribalski[8], Jonathan Davies[9], Elias Brinks[10], W. J. G. de Blok[11], Mary E. Putman[12], and Wim van Driel[13]

[1] Department of Physics, Engineering Physics and Astronomy, Queen's University, Kingston, ON K7L 3N6, Canada; irwin@astro.queensu.ca
[2] Department of Physics, Lafayette College, Easton, PA 18042, USA; hoffmang@lafayette.edu
[3] Department of Physics, Royal Military College of Canada, P.O. Box 17000, Station Forces, Kingston, ON K7K 7B4, Canada; kristine.spekkens@rmc.ca
[4] Center for Radiophysics and Space Research, Cornell University, Ithaca, NY 14853, USA; haynes@astro.cornell.edu, riccardo@astro.cornell.edu
[5] Hamburger Sternwarte, Universität Hamburg, Gojenbergsweg 112, D-21029 Hamburg, Germany; suzanne.linder@hs.uni-hamburg.de
[6] Max-Planck-Institut für Astrophysik, D-85748 Garching, Germany; bcatinel@MPA-Garching.mpg.de
[7] NAIC-Arecibo Observatory, HC3 Box 53995, Arecibo, PR 00612, USA; emomjian@naic.edu
[8] Australia Telescope National Facility, CSIRO, Epping, NSW 1710, Australia; Baerbel.Koribalski@csiro.au
[9] School of Physics and Astronomy, Cardiff University of Wales, Cardiff CF24 3YB, UK; jonathan.davies@astro.cf.ac.uk
[10] Centre for Astrophysics Research, Science and Technology Research Institute, University of Hertfordshire, Hatfield AL10 9AB, UK; ebrinks@star.herts.ac.uk
[11] Department of Astronomy, University of Cape Town, Rondebosch 7700, South Africa; edeblok@ast.yct.ac.za
[12] Department of Astronomy, Columbia University, New York, NY 10027, USA; mputman@astro.columbia.edu
[13] Observatoire de Meudon, 5 Place Jules Janssen, 92195 Meudon, France; wim.vandriel@obspm.fr
Received 2008 August 14; accepted 2008 September 25; published 2009 February 24

ABSTRACT

We have conducted a deep, complete H I survey, using Arecibo/Arecibo L-band Feed Array (ALFA), of a field centered on the nearby, isolated galaxy, NGC 2903, which is similar to the Milky Way in its properties. The field size was 150 kpc × 260 kpc and the final velocity range spanned from 100 to 1133 km s^{-1}. The ALFA beams have been mapped as a function of azimuth and cleaned from each azimuth-specific cube prior to forming final cubes. The final H I data are sensitive down to an H I mass of $2 \times 10^5 M_\odot$ and column density of 2×10^{17} cm^{-2} at the $3\,\sigma\,2\,\delta\,V$ level, where σ is the rms noise level and $\delta\,V$ is the velocity resolution. NGC 2903 is found to have an H I envelope that is larger than previously known, extending to at least three times the optical diameter of the galaxy. Our search for companions yields one new discovery with an H I mass of $2.6 \times 10^6\ M_\odot$. The companion is 64 kpc from NGC 2903 in projection, is likely associated with a small optical galaxy of similar total stellar mass, and is dark matter dominated, with a total mass $>10^8\ M_\odot$. In the region surveyed, there are now two known companions: our new discovery and a previously known system that is likely a dwarf spheroidal, lacking H I content. If H I constitutes 1% of the total mass in all possible companions, then we should have detected 230 companions, according to Λ cold dark matter (ΛCDM) predictions. Consequently, if this number of dark-matter clumps are indeed present, then they contain less than 1% H I content, possibly existing as very faint dwarf spheroidals or as starless, gasless dark-matter clumps.

Key words: dark matter – galaxies: individual (NGC 2903) – galaxies: formation – galaxies: spiral – radio lines: ISM

Online-only material: color figures

1. INTRODUCTION

Weak gravitational lensing studies have shown that stellar light traces dark matter on supercluster and cluster scales (Heymans et al. 2008). The issue is much less clear on subgalactic scales, however, as evidenced by the well known "missing satellites" problem around the Milky Way (MW). At issue is the fact that the predicted number of satellites based on cold dark matter (CDM) and Λ cold dark matter (ΛCDM) simulations of galaxy formation is significantly greater than the observed number of dwarf MW companions (Kauffmann et al. 1993; Klypin et al. 1999; Moore et al. 1999; Diemand et al. 2007b).

A number of explanations for this discrepancy have been proposed. These include the suppression of star formation due to the ionization of the gas (Barkana & Loeb 1999; Benson et al. 2002; Shaviv & Dekel 2003; Gnedin et al. 2008) or dissociation of molecular hydrogen (Haiman et al. 1997), gas stripping due to supernovae-driven winds from an early star formation epoch (Hirashita et al. 1998; Klypin et al. 1999), only the most massive halo substructures forming stars (Stoehr et al. 2002), the disruption of satellites by tidal stripping/stirring (Klypin et al. 1999; Mayer et al. 2001a, 2001b; Kravtsov et al. 2004), confusion between dwarf satellites and high-velocity clouds (HVCs, see Klypin et al. 1999 for a summary), the suppression of small-scale power in simulations via contributions from warm dark matter (Avila Reese et al. 2001; Zentner & Bullock 2002), and incompleteness in the census of MW satellites (Mateo 1998).

It is now clear that the latter explanation has played a part, since in the past few years, the known population of dwarf MW satellites has almost doubled based on scrutiny of the Sloan Digital Sky Survey (SDSS; York et al. 2000, see also Koposov et al. 2008); however, although the detection of the new satellites alleviates the problem, it does not eliminate it entirely since, after making corrections for sky coverage, the discrepancy is still approximately a factor of 4 (see Simon & Geha 2007).

The concept that star formation might, in some way, have been suppressed in systems of low total mass, suggests the possibility that dark-matter substructure could still be traced by atomic hydrogen (H I) even though appreciable stellar content

[14] National Astronomy and Ionosphere Center, Cornell University, Ithaca, NY, 14853, USA.
[15] NAIC-Arecibo Observatory, HC3 Box 53995, Arecibo, PR, 00612, USA.
[16] NRAO, PO Box O, Socorro, NM, 87801, USA.

may be missing. However, many searches, with a variety of sensitivity and coverage, have been undertaken for low-mass starless companions, with little success (see Section 2) and some have suggested that small galaxies which retain H I are likely to have developed stars as well (Briggs 2004; Taylor & Webster 2005).

The advent of the seven-beam Arecibo L-band Feed Array (ALFA; see Giovanelli et al. 2005a)[17] has now provided an opportunity to survey nearby systems for the possible presence of such "dark companions," with unprecedented sensitivity, coverage, and speed. We report here the results of a targeted deep survey of a single, isolated galaxy, NGC 2903 (see Section 3). In this paper, we outline our observational procedure and data reduction, we present global results for NGC 2903 and then concentrate on companions and their implications for primordial dark matter searches. The details of the H I in NGC 2903, itself, will be left for a subsequent paper. Please note that data related to this project, including some software that we have developed, data from related observations, our final cubes and beam maps can be found on our NGC 2903 Web site.[18]

In Section 2, we outline previous surveys that have taken place, presenting a comparison with our approach and, in Section 3, we discuss NGC 2903 and its environment. Since this paper introduces new techniques for observing and reducing Arecibo/ALFA data, we discuss these in detail in Sections 4 and 5. Our detection thresholds and data quality are given in Section 6, Section 7 presents the results for NGC 2903 and its environment, and Sections 8 and 9 provide the discussion and conclusions, respectively.

2. PREVIOUS H I SURVEYS AND COMPARISON WITH NGC 2903

Current observational data suggest that H I clouds tend not to be "intergalactic," but rather associated with galaxies (Briggs 2004). Various searches for faint H I around galaxies, however, have typically been hampered by the need to choose sensitivity at the expense of coverage or vice versa.

For wide coverage, the blind H I Parkes All Sky Survey (HIPASS; Barnes et al. 2001; Koribalski et al. 2004; Meyer et al. 2004) revealed only one definite extragalactic H I cloud in the NGC 2442 group with a high H I mass of about 10^9 $M_\odot$ (Ryder et al. 2001). This cloud has been interpreted as a remnant of a tidal interaction (Bekki et al. 2005) and cannot be considered primordial.

As for targeted searches, lower mass limits have been achieved. Zwaan (2001) and de Blok (2002) made incomplete samplings of several galaxy groups to limits of a few $\times 10^6 M_\odot$. Minchin et al. (2003) surveyed the Cen A group to a limit of 2×10^6 $M_\odot$, and Pisano et al. (2004, 2007) observed six Local Group analogs to (2–5) $\times 10^6$ $M_\odot$. Kovac et al. (2005) completely surveyed the Canes Venatici group to a limit of 10^6–10^7 $M_\odot$. Barnes & de Blok (2004) searched for faint H I companions around NGC 1313 and Sextans A to $\sim 10^6$ $M_\odot$. Pisano & Wilcots (1999, 2003) searched for gas rich companions around six isolated galaxies to an approximate detection limit of only $10^8 M_\odot$.[19] In these and other targeted surveys (see also Kilborn et al. 2006), neither starless H I companions nor HVCs, where the sensitivity was sufficient (e.g., Zwaan & Briggs 2000; Pisano et al. 2007), were detected with the exception of H I that could again be attributed to tidal debris (e.g., see Bekki et al. 2005).

In contrast to the targeted searches described above, our study of a relatively isolated system (see Section 3) simplifies the interpretation of any H I detections since tidal explanations are much less likely. Moreover, use of the 305 m diameter Arecibo radio telescope has placed these observations among the most sensitive yet achieved (see Section 6.1). While slightly lower H I mass limits have been claimed in deep interferometric observations of NGC 891 (Oosterloo et al. 2007), M 31, and M 33 (Westmeier et al. 2005a), our combination of low-mass detection limits, the lowest H I column density limits yet achieved in such studies, the sensitivity to broad scale structure not possible via interferometers, and the complete (and large) sky coverage combine to make this survey unique.

3. NGC 2903 AND ITS ENVIRONMENT

NGC 2903 (Table 1 and Figure 1) has a number of assets that make it a good target for deep H I mapping. It falls within the declination range of the Arecibo telescope, it is bright and massive so there is a reasonable expectation of the presence of ΛCDM (or other) satellites, it is of large angular size so is easily resolved by the Arecibo beam, it is nearby yet lies beyond the Local Group ($D = 8.9$ Mpc; Drozdovsky & Karachentsev 2000; $1' = 2.6$ kpc[20]), and some previous H I observations of the galaxy are available for comparison (Begeman 1987; Begeman et al. 1991; Hewitt et al. 1983; Haynes et al. 1998). An important characteristic is that it is noninteracting and isolated, in the sense that no galaxies larger than one quarter of its optical size are present within 20 optical diameters away (No. 0347 in the Catalog of Isolated Galaxies; Karachentseva 1973;[21] see also Haynes et al. 1998).

NGC 2903 is characterized by its barred, grand-design spiral pattern. It displays a number of "hot spots" in its nuclear region as well as a ring of star formation (e.g., Pérez-Ramírez et al. 2000). The nuclear dust distribution is chaotic (Martini et al. 2003). The CO emission is concentrated along the bar (Regan et al. 1999) and the star formation rate (SFR) per unit area is enhanced by an order of magnitude in the nucleus in comparison to the disk (Jackson et al. 1991). A soft X-ray halo extending to the west of the nucleus has been interpreted as outflow from a nuclear starburst-driven wind (Tschöke et al. 2003).

Aside from evidence of nuclear star formation, however, NGC 2903 is a typical massive spiral whose properties are similar to those of the MW. Its global SFR (2.2 $M_\odot$ yr^{-1}; Table 1) is comparable to the MW value (~ 4 $M_\odot$ yr^{-1}; Diehl et al. 2006), considering the different methods for estimating this value. More importantly, its rotation curve shows a rise to 210 km s^{-1} at a galactocentric radius of $R \sim 4$ kpc, declining slightly to 180 km s^{-1} by $R \sim 33$ kpc, its outermost measured point (Begeman et al. 1991). These values agree with the rotation curve of the MW over $4 \leqslant R$ (kpc) $\leqslant 33$ to within error bars (Xue et al. 2008). Aside from environment, therefore, NGC 2903 appears to be an analog of the MW.

As indicated above, NGC 2903 is considered to be an isolated galaxy, given the dearth of nearby companions sufficiently massive to perturb it. However, two small companions, UGC

[17] See also http://www.naic.edu/alfa/.
[18] http://www.astro.queensu.ca/~irwin/ngc2903.
[19] Note that the various groups have not all used the same criteria for determining their mass limits.
[20] Literature values range from 6.01 Mpc to 11.65 Mpc, depending on corrections for local motions (see the NASA/IPAC Extragalactic Database (NED)).
[21] At the time of writing, NGC 2903 has not been included in the Analysis of the interstellar Medium of Isolated Galaxies (AMIGA) catalog (e.g., Verley et al. 2007) due to its large angular size.

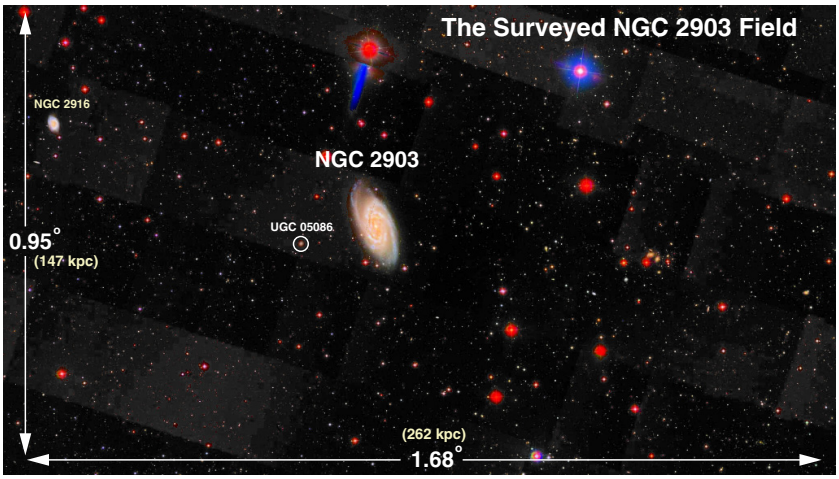

Figure 1. SDSS DR6 image of the field around NGC 2903 that has been surveyed by the Arecibo telescope. NGC 2903 and its companion, UGC 5086, are labeled, as well as the scale. The background galaxy, NGC 2916, is also labeled (see Section 7.2).

(A color version of this figure is available in the online journal.)

Table 1
Parameters of NGC 2903[a]

Parameter	NGC 2903
R.A. (h m s)	09 32 10.11
decl. (° ′ ″)	21 30 03.0
Type	SB(s)d
$V_\odot$ (km s^{-1})[b]	556.0
D (Mpc)[c]	8.9
2a × 2b (′ × ′)[d]	12.6 × 6.0
(kpc × kpc)	32.6 × 15.5
L_{FIR} (10^{10} $L_\odot$)[e]	1.30
L_{IR} (10^{10} $L_\odot$)[e]	1.80
SFR ($M_\odot$ yr^{-1})[f]	2.2

Notes.
[a]Data from NED unless otherwise indicated.
[b]Heliocentric velocity.
[c]Drozdovsky & Karachentsev (2000).
[d]Optical major × minor axis diameters. The semi-major diameter, a, is equivalent to R_{25}, the radius in the B band at the 25.0 mag arcsec^{-2} isophote level.
[e]Infrared and far-infrared luminosity (Sanders et al. 2003), adjusted to our distance.
[f]SFR from L_{FIR} and the formalism of Kennicutt (1998).

Table 2
Companion Galaxies of NGC 2903[a]

Parameter	UGC 5086[b]	D565-06[c]	D565-10[c]
R.A. (h m s)	9 32 48.9	9 19 30.0	9 30 12.8
decl. (° ′ ″)	21 27 55	21 36 12	19 59 26
Sep. (′)[d]	9.3	176.8	94.7
(kpc)[d]	24	458	245
$V_\odot$ (km s^{-1})[e]	510 ± 30[f]	498 ± 2	562 ± 1
2a × 2b (′ × ′)[g]	0.9 × 0.9	0.7 × 0.6	0.7 × 0.6
Mag.[h]	18	16.95	17.0
Ref.[i]	DK00	DK00	this work

Notes.
[a]Data from NED unless otherwise indicated.
[b]Alternate names: D565-05 in the Low Surface Brightness Galaxy Catalog (LSBC); J093248.81+212756.2 in the SDSS.
[c]Identifier in the LSBC.
[d]Projected separation from the center of NGC 2903.
[e]Heliocentric radial velocity.
[f]Optical velocity, cz, as given in the SDSS Data Release 6 (DR6).
[g]Major axis × minor axis diameters.
[h]Optical B magnitude.
[i]Reference for association with NGC 2903. DK00 = Drozdovsky & Karachentsev (2000).

5086 and D565-06, are known to be associated (Drozdovsky & Karachentsev 2000) and, from an optical search for additional possible companions within similar radii, we have now identified a third companion, D565-10. D565-10 was found from a search over the spatial region and velocity range within which UGC 5086 and D565-06 have previously been found. Since its separation from NGC 2903 in both position and velocity space is less than that of D565-06, we include it as a newly identified companion here. These three galaxies and their known properties are listed in Table 2. Of the three, only UGC 5086 is within our surveyed field of view and is labeled in Figure 1.

Aside from the H I observations listed above, more recent H I data from the HIPASS (Wong et al. 2006) and the Westerbork SINGS survey (Braun et al. 2007) are now also available. NGC 2903 is also in The H I Nearby Galaxy Survey (THINGS, Walter et al. 2008) which makes use of Very Large Array (VLA) data. At the time of our observations, five archival VLA unpublished H I data sets were available, all of which we have reduced. Of these, two sets produced good data. These are: (1) observing run AO125, taken 1996 September 29 constituting 2.03 hr on source in D configuration, and (2) run AW536, taken 2000 April 22, constituting 2.68 hr on source in C configuration. We do not reproduce the VLA cubes here, but make them available on our NGC 2903 Web site,[18] and refer to them, as needed, only for comparison purposes. The VLA data sets are of higher spatial resolution than the Arecibo/ALFA data, but are much less sensitive (see Section 7.1.2, for example). These reference VLA data sets predate those of THINGS.[22]

4. OBSERVATIONS

Observations were carried out with the 305 m telescope of the Arecibo Observatory[23] using the seven-beam ALFA receiver

[22] The THINGS data set achieves a sensitivity of $N_{HI} = 4 \times 10^{19}$ cm^{-2} at a resolution of 30 arcsec, using the same criteria as we will set out in Section 6.
[23] The Arecibo Observatory is part of the National Astronomy and Ionosphere Center (NAIC), a national research center operated by Cornell University under a cooperative agreement with the National Science Foundation (NSF).

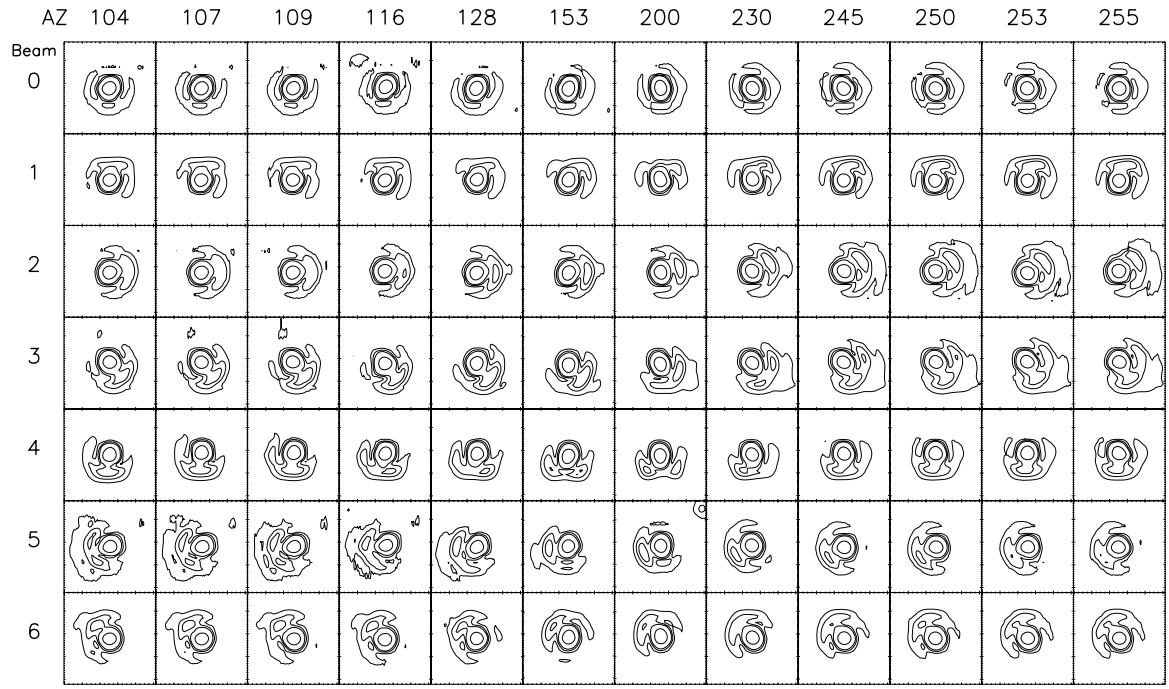

Figure 2. Maps of each ALFA beam (rows) used to deconvolve sidelobe and stray radiation contributions from NGC 2903 observations at each azimuth (columns). Each panel spans 24′ in both R.A. and decl., and contours are at (−18, −12, −9, −3) dB. See Figure 2 of Giovanelli et al. (2005a) for an illustration of the beam locations in the ALFA footprint. FITS files containing the 84 beams may be downloaded from our Web site.

system (see Figure 2 of Giovanelli et al. 2005a, for the ALFA beam geometry) with the Wideband Arecibo Pulsar Processor (WAPP) back-end spectrometer system. The total observing time allocated for this project was 97 hours, divided into 37 observing blocks (2004 November 28–30, December 1–6, 14–23, 26; 2005 February 10–13, 28, March 1–6, 21–26) carried out during the commissioning phase of ALFA. The observing setup is summarized in Table 3.

Because the ALFA beams can have coma lobes as high as 20% (7 dB), high-sensitivity observations of extended objects with this instrument must account for contributions from stray/unwanted radiation into these lobes; that is, we obtain a "dirty map" which must be "cleaned." Our basic approach is therefore to map the field in Figure 1 as well as the seven ALFA beams in a fixed number of telescope configurations. The beam maps are used to deconvolve the sidelobe contribution to the galaxy map in each configuration after which these clean maps are combined to form our final datasets. In Sections 4.1 and 4.2, we describe our observing strategy for mapping the galaxy and the beams, respectively.

4.1. Observations of NGC 2903

The mapping of NGC 2903 was conducted in a "Fixed Azimuth Drift" mode similar to that adopted in the Arecibo Galaxy Environment Survey (AGES; Auld et al. 2006).[24] It is, however, somewhat less efficient than the dual-pass strategy employed by the Arecibo Legacy Fast ALFA Survey (ALFALFA; Giovanelli et al. 2005a),[25] mainly because we observed NGC 2903 at 12 separate azimuths in order to increase the effective integration time per point to 6 times the ALFALFA value.

For each of 12 azimuths ($AZ = 104°, 107°, 109°, 116°, 128°, 153°, 200°, 230°, 245°, 250°, 253°, 255°$), ALFA was positioned to point 4^m in R.A. ahead of the source, then held motionless while the source drifted through. Spectra for each linear polarization of each of the seven feeds were recorded at a rate of once per second during the drift scan. Thus 12 drift scans centered at a single declination could optimally be obtained in one observing session. The azimuths were determined by calculating the minimum time required for slewing and resetting/adjusting system parameters in preparation for the next drift at the next azimuth, thus minimizing overheads.

Before each drift scan at each azimuth, the ALFA turret was rotated so as to produce equal separations in declination between successive beams (but see below). The azimuth and zenith angle were also both adjusted so that a drift would cross the same declination (J2000) any time it was repeated.

On a given night, drifts at all 12 azimuths kept the center beam of ALFA at the same declination. On following nights, the declination was shifted by 4′45″ so that the center beam drifted through the interstice between the northermost beam of the preceding night's drift and the southernmost of the following.

Table 3
Observing Setup

Parameter	Value
Galaxy	
Bandwidth (MHz)	12.5
Center frequency, ν_c (GHz)	1.417
No. channels	2048
Velocity coverage (km s^{-1})[a]	−585.5 → 2064.2
Channel width (km s^{-1})	1.293
Drift scan duration (s)	480
Beams	
Bandwidth (MHz)	50.0
Center frequency (GHz)	1.405
Drift scan duration (s)	240

Note. [a] All velocities in this paper are heliocentric.

[24] http://www.naic.edu/~ages.
[25] http://egg.astro.cornell.edu/alfalfa/.

This helped to produce a map with as uniform a sensitivity as possible and Nyquist sampled the survey area in declination.

In the allocated time we were able to obtain full sets of 12 drifts each, across 13 nearly constant declination tracks with the center beam spanning 21°03′56″ to 22°00′56″ (J2000), and with another full set of 12 drifts spanning 21°13′26″ to 21°27′41″ and 21°37′11″ to 21°51′26″. We refer to the number of drifts at a given declination as N_p. Compared to these repeated drift ranges, our final map is undersensitive in the central declination strip 21°32′26″, the two southernmost strips and the two northernmost strips (see Section 6.1 for sensitivity).

The Fixed Azimuth Drift mode introduces some variations in declination. First of all, since the telescope was held at fixed azimuth and zenith angle through each drift, the declination tracked by each beam changed by a small amount from the start to the end of the drift. We have computed the average variation in beam position from this effect, and find it to be less than 1 arcsec and therefore negligible. Secondly, the declination spacing between ALFA beams at a given azimuth was not exactly uniform. The variation in beam spacing is typically $\approx 2\%$ of the beam size, a value comparable to the $\approx 5''$ pointing accuracy of the Arecibo telescope. Finally, the declination spacings vary with azimuth due to the elliptical illumination pattern of the Arecibo telescope. These declination separations varied monotonically from $\sim 123''$ $AZ = 180°$ to $\sim 108''$ at $AZ = 104°$ and $AZ = 255°$. We account for the latter two effects in the data reduction (see Section 5.1).

4.2. Beam Mapping

The outer beams of ALFA have significant coma lobes, and the contributions of stray radiation and outer sidelobes to all the beams is not negligible. While precise beam maps were produced by G. Cortés (2003, private communication), they do not account for variations with azimuth and zenith angle or blockage by the platform and cables.

Consequently it was necessary to map the beams by observing strong unresolved continuum sources using a mapping strategy similar to that described in Section 4.1. In the case of the beams, however, we chose twice as many azimuth settings (24 instead of 12) and shorter drift scans (Table 3).

The declination of Beam 0, which is the center beam of ALFA, was shifted by 1′53″ (about half a beamwidth) from one night to the next, and we completed 13 separate drifts on each source. No single source of sufficient strength could be mapped at each of the 24 azimuths in the time we were allotted on any one night, so we mapped two of them: J080538+210651 (0.9 Jy) at $AZ \lesssim 120°$ and J102155+215931 (1.7 Jy) at $AZ \gtrsim 120°$.

This procedure gave us beam maps approximately 56′ long in R.A. and spanning 23′ in decl. Only Beam 0 is mapped to equal distances north and south of the center, however. While the span in R.A. is sufficient to map the first several sidelobes of each of the outer beams, the span in declination falls short of reaching the second sidelobe for the northernmost and southernmost beams. This will be discussed further in Section 5.2.

5. DATA REDUCTION AND PROCESSING

The drift scans were bandpass subtracted and baseline flattened using IDL procedures written by P. Perillat for general use at Arecibo Observatory, and by R. Giovanelli and B. R. Kent for the ALFALFA precursor data (Giovanelli et al. 2005b). Preliminary calibration was accomplished using the system's equivalent flux density for each beam as a function of zenith angle, provided by Arecibo Observatory staff. Data reduction specific to the galaxy and beams is described below.

5.1. Galaxy Data Reduction

Initial maps of NGC 2903 from the drifts showed significant striping across the galaxy, indicating that the calibration of the individual beams was not sufficiently precise. An attempt to improve the calibration by integrating over the Galactic H I emission, requiring the integral to be the same for each beam, proved unsuccessful since the separate beams follow different tracks across the Galactic emission and, on the scale of the NGC 2903 map, there is significant variation of the Galactic H I emission between those tracks.

To improve the calibration, we sought to make use of the continuum sources in the mapped field. Sources with sizes small compared to the Arecibo beam and with peak flux densities exceeding 10 mJy were selected from NED. Gaussians were fitted to corresponding detected continuum signals in our data, the distance from the fitted peak to the cataloged source position was determined, and the ratio of the flux expected at that position to that observed was calculated. Only detections that fell within half a beamwidth of the source were used. Starting with the strongest source, then working down the list in order of source strength, the factors by which each beam must be multiplied to place their gains on a common scale were determined. The resulting calibration is referenced to the flux of the strongest source in the field, J093215+211243, which we took to have peak flux density 562.3 mJy at the time of our observations. This approach significantly reduced the striping in the final maps, though we note the presence of residuals that will be discussed in Section 6.2.

The drifts for each azimuth separately were then gridded into a datacube with axes, right ascension (R.A.), declination (decl.), and velocity (V). This was done using the ALFALFA IDL gridding tool (R. Giovanelli et al. 2008, in preparation) modified for the NGC 2903 drift length and calibration method. At each defined point in the grid, the gridding tool produced a weighted average of emission from nearby 1 s spectral samples, using the positions recorded in the data headers for each. No assumption of constant separation in declination from one beam to the next was required in this process. The beam which dominated the weight for each grid point was also recorded in the data structure, for use later by the cleaning software (see Section 5.3). The grid pixel size was 30″ in R.A. and decl., and the velocity range was chosen to extend well beyond that of NGC 2903, excluding Galactic emission.

There was no significant radio frequency interference from outside the observatory in our spectra. However, there was an internally generated "wandering birdy" (Giovanelli et al. 2005b) present in some of our drifts. This was an interference spike that drifted nonmonotonically in frequency during particular drifts. The source has since been identified and corrected, and has not been seen in any observations since early 2005, to our knowledge. Fortunately the birdy's wanderings did not take it close to the NGC 2903 velocity range during our observations for the most part. In those few spectra where it would have caused difficulty in the cleaning process, it was excised by interpolating between spectral channels just outside the spike.

5.2. Beam Data Reduction

To produce a separate two-dimensional (2D) map of each beam at each azimuth, we extracted the individual beam drifts

from the sets of drift scans, then constructed maps of the continuum source as seen by each beam, producing seven maps for each of the 24 azimuth settings. The continuum maps were written out from IDL into Flexible Image Transport System (FITS) format, then read into the Astronomical Information Processing System software, aips++,[26] of the National Radio Astronomy Observatory (NRAO). Standard 2D Gaussian fitting routines in aips++ were used to fit and subtract out each cataloged continuum point source outside the much stronger target source. Noticeable sidelobe signal from these nontarget sources was zeroed as well, as long as there was no confusion with the sidelobes of the target source. Our inability to completely erase these extraneous sources limits the dynamic range of the final galaxy maps (see Section 6.2).

These maps were then read into the Astronomical Image Processing System (AIPS)[27] for further processing. The goal was to create a single map for each of the seven beams at each of the 12 galaxy azimuths (84 beam maps in total). To do this, the beam maps were placed on the same amplitude scale and beam maps at azimuths adjacent to the galaxy azimuth were averaged together, weighted by distance from the galaxy azimuth. For example, beam maps at $AZ = 103^\circ$ and $AZ = 106^\circ$ were averaged to obtain an estimate of the beam at the galaxy azimuth $AZ = 104^\circ$, with a higher weight attributed to $AZ = 103^\circ$.

The final beam maps at each galaxy azimuth covered $54'$ in R.A. and $21'$ in decl. This was more than sufficient to fully map the beam shape in right ascension. However, as indicated in Section 4.2, the declination span does not reach the second sidelobe for the northernmost and southernmost beams. In addition, for four of the seven beams, the first sidelobe on one side only was cut off in declination at approximately the midpoint of its peak. For these cases, to avoid the introduction of artifacts during the deconvolution process (Section 5.3), the beam sidelobe was extended/smoothed at the edge by a Gaussian of width, $2'.3$.

All 84 beams are displayed in Figure 2 and nicely show the changing beam structure with changing azimuth.[28] These beams were then used for the IDL-based clean described in the next section.

5.3. Image Deconvolution and Final Cubes

To achieve high sensitivity to low-level emission from the outer edges of the galaxy it is necessary to remove the sidelobe and stray radiation contribution to the maps of NGC 2903. We perform this deconvolution with a "clean" algorithm analogous to that used in aperture synthesis imaging (see Cornwell et al. 1999, for a review).

We use an image-plane IDL-based implementation of the clean algorithm written by Buie (2008), modified by us to account for the multiple beams.[29] Since the dominant contributing beam was recorded in the grid data structure for each point, we were able to calculate the contribution to that point from a point source anywhere in the R.A.–decl. map at each velocity. Each iteration consisted of identifying the strongest remaining emission in the map, then using the appropriate known beams to remove the contributions of that point to the entire map. Iterations continued until the first negative clean component was reached, or until the clean component reached the level of the noise which we took to be 2 mJy. This clean procedure was carried out at each azimuth, producing 12 cleaned NGC 2903 data cubes.

The cleaned cubes were then read into AIPS for further reduction and analysis. Each of these cubes was inspected individually and some minor editing (e.g., of remaining wandering birdie spikes farther from the galaxy emission) was carried out. All cubes at different azimuths were then averaged to form a single cube. A subset of velocity space in the cube was then extracted so as to avoid noisy end channels as well as contaminating Galactic emission on the low-velocity side. The resulting full-resolution cube will be designated as the "Original" cube. This cube was then smoothed, in velocity alone (denoted V-smoothed), spatially alone (RD-smoothed) and both spectrally and spatially (RDV-smoothed). The spatial smoothing, in particular, ameliorates the striping issue discussed in Section 5.1, improving the rms noise in the maps (see next section). Finally, residual curvature in the baseline was removed, point by point.[30] The parameters of the final cubes are given in Table 4, and the cubes themselves may be obtained from our Web site.

6. DETECTION LIMITS AND DATA QUALITY

A selection of R.A.–V plots and R.A.–decl. plots of the final cubes are shown in Figures 3 and 4, respectively. The grayscale in the plots emphasizes low-intensity emission to illustrate the data sensitivity in low dynamic range regions of the cube as well as residual map errors near NGC 2903. We discuss these map properties in turn below.

6.1. Data Sensitivity

The mean, $\bar{S}$, and rms noise, σ, of all regions beyond the extended envelope of NGC 2903 (see Section 7.1) in each cube is listed in Table 4. As expected in these low dynamic range regions, the final baseline is consistent with zero ($\bar{S} \ll \sigma$) and a histogram of σ over all line-free channels is Gaussian.

The variation in σ as a function of right ascension, declination, and V was examined. While we find that σ is independent of R.A. and V, it does vary with declination, a result that is illustrated in Figure 5(a). This is primarily caused by the higher gain of the central beam, Beam 0 ($\sim$ 11 K Jy^{-1}) relative to the outer ones ($\sim$ 8.5 K Jy^{-1}). The result is that declinations surveyed with the former have lower σ. The correspondence between the declination of Beam 0 for each drift (location of points along x-axis of Figure 5(d)) and the minima in Figure 5(a) illustrates this effect. Different numbers of drift scans at some declinations (Figure 5(d)), uncertainties in beam calibration and variations in beam spacing (see Section 4.1) also contribute to changes in σ with declination.

From the noise values and some assumptions, we can compute detection limits for each cube in the low dynamic range regime. We consider the limiting flux integral, $\mathcal{S}_{\rm lim}$, to be from an unresolved signal that is at a 3σ level in two independent channels,

$$\mathcal{S}_{\rm lim} = 3\sigma\, 2\delta V \text{ Jy km s}^{-1}, \quad (1)$$

where δV (km s^{-1}) is the velocity resolution (see Table 4) and σ is in Jy beam^{-1}. The minimum detectable H I mass is then,

$$M_{\rm HI\,lim} = 2.356 \times 10^5\, D^2\, \mathcal{S}_{\rm lim}\, M_\odot \quad (2)$$

[26] http://aips2.nrao.edu.
[27] http://www.aips.nrao.edu/.
[28] FITS files for these beams are available on the NGC 2903 Web site.
[29] See mbmclean.pro on our Web site.
[30] The AIPS task, XBASL, was used.

Table 4
Parameters of Cubes

Parameter	Original	*V*-smoothed	RD-smoothed	RDV-smoothed
Final velocity coverage (km s^{-1})[a]	100.0 → 1132.8	100.0 → 1132.8	100.0 → 1132.8	100.0 → 1132.8
Channel width (km s^{-1})	1.293	1.293	1.293	1.293
Velocity resolution, δV (km s^{-1})[b]	2.59	5.17	2.59	5.17
Spatial resolution, θ (arcsec)[c]	234	234	270	270
σ (mJy beam^{-1})[d]	1.1	0.80	0.61	0.44
Mean (mJy beam^{-1})[e]	0.0069	0.0069	0.00988	0.00983
$M_{\rm HI\,lim}$ ($M_\odot$)[f]	3.2×10^5	4.7×10^5	1.8×10^5	2.6×10^5
$N_{\rm HI\,lim}$ (cm^{-2})[g]	3.5×10^{17}	5.1×10^{17}	1.5×10^{17}	2.1×10^{17}
Max S/N[h]	533	730	1076	1475

Notes.
[a]Bandwidth range after removing end channels and Galactic emission.
[b]Since Hanning smoothing was applied, the original velocity resolution is not equivalent to the channel width.
[c]Full width at half maximum of the Gaussian beam.
[d]rms noise over all regions of the cubes in which the galaxy emission had been blanked.
[e]Mean over all regions of the cubes in which the galaxy emission had been blanked.
[f]H I mass limit ($3\,\sigma\,2\delta\,V$, as described in Section 6.1).
[g]H I column density limit ($3\,\sigma\,2\delta\,V$, as described in Section 6.1).
[h]Maximum signal-to-noise (S/N) ratio of each cube. The S/N cubes are described in Section 6.1.

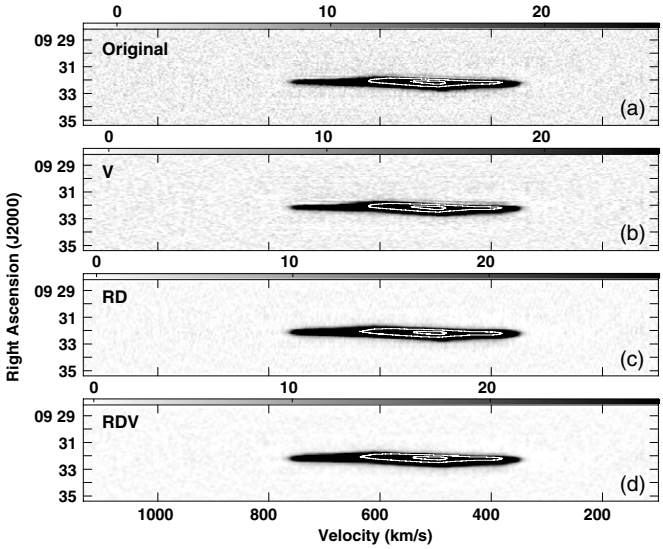

Figure 3. Right ascension–velocity plots at decl. = 21°30′03″, for the Original cube (a), the V-smoothed cube (b), the RD-smoothed cube (c), and the RDV-smoothed cube (d) (see Table 4). *V* is indicated at the bottom of the lowest frame. In each case, the grayscale range, marked at the top of each frame, goes from -1σ to 10% of the maximum in the frame, the latter being 253.0 mJy beam^{-1} for (a), 252.1 mJy beam^{-1} for (b), 285.9 mJy beam^{-1} for (c), and 284.5 mJy beam^{-1} for (d). Contours at 50% and 90% of the peak are also shown.

where D is the distance (Mpc), and the minimum detectable column density for a signal that uniformly fills the beam is

$$N_{\rm HI\,lim} = \frac{2.228 \times 10^{24}}{(\theta\ \nu_c)^2}\ \mathcal{S}_{\rm lim}\ {\rm cm}^{-2}, \qquad (3)$$

where θ is the spatial resolution (arcsec, Table 4) and ν_c is the central frequency (GHz, Table 3). If the signal does not uniformly fill the beam, then the right-hand side of Equation (3) must be divided by an areal filling factor.

Plots of $M_{\rm HI\,lim}$ and $N_{\rm HI\,lim}$ as a function of decl. are shown in Figures 5(b) and (c), respectively, and the mean values for each cube are given in Table 4. Note that the cubes smoothed in velocity have higher $M_{\rm HI\,lim}$ and $N_{\rm HI\,lim}$ than their full-resolution counterparts because of the larger δV of the former. Note also that these results are simply detection limits for the data, without imposing assumptions about the properties of any companions that might be present. The limits shown in Table 4 are very low; for example, the column density limits are lower than those of THINGS by two orders of magnitude.[22]

6.2. Residual Map Errors near NGC 2903

Close inspection of Figures 3 and 4 reveal residual map errors near NGC 2903 that remain even after the data reduction procedure discussed in Section 5. These artifacts, described below, limit the dynamic range of the data in regions occupied by emission from NGC 2903 itself, having a greater relative effect near the "edges" of this emission.

One artifact that is evident in Figures 3(a) and (b) is a faint ridge of emission seen on the low-RA side of the galaxy emission, running close to and parallel with the "edge" of the main galaxy emission. This ridge is due to imperfectly cleaned sidelobes (see Section 5.2). It is most evident in the data at full spatial resolution, and occurs at typically a 2–5% level in comparison to the brightest galactic emission at the same velocity.

Another type of artifact is evident in Figures 4(a) and (b), and can be attributed to residual striping due to scan calibration uncertainties (Section 5.1). These residual errors vary in strength but are typically at the level of a few percent of the peak in any given channel near the edge of the main emission. They produce the "scalloping" of the edges of the H I distribution in NGC 2903 at low column densities.

Finally, the second sidelobes (outer coma lobes) of the beams were not fully mapped in declination, thus limiting the effectiveness of the cleaning in this dimension (see Section 5.2). From an examination of the rather complex outer lobes observed in right ascension, we estimate that second sidelobe peaks at approximately 0.6% of the central beam peak could contribute to emission as far as 10′ away in declination (note, however, that this varies beam to beam and azimuth to azimuth).

Considering these residual map errors and typical peak H I flux densities measured for NGC 2903 in our data, we caution against simple interpretations of emission below a few percent in any given channel over the emission region occupied by NGC 2903 itself. We estimate that a more conservative

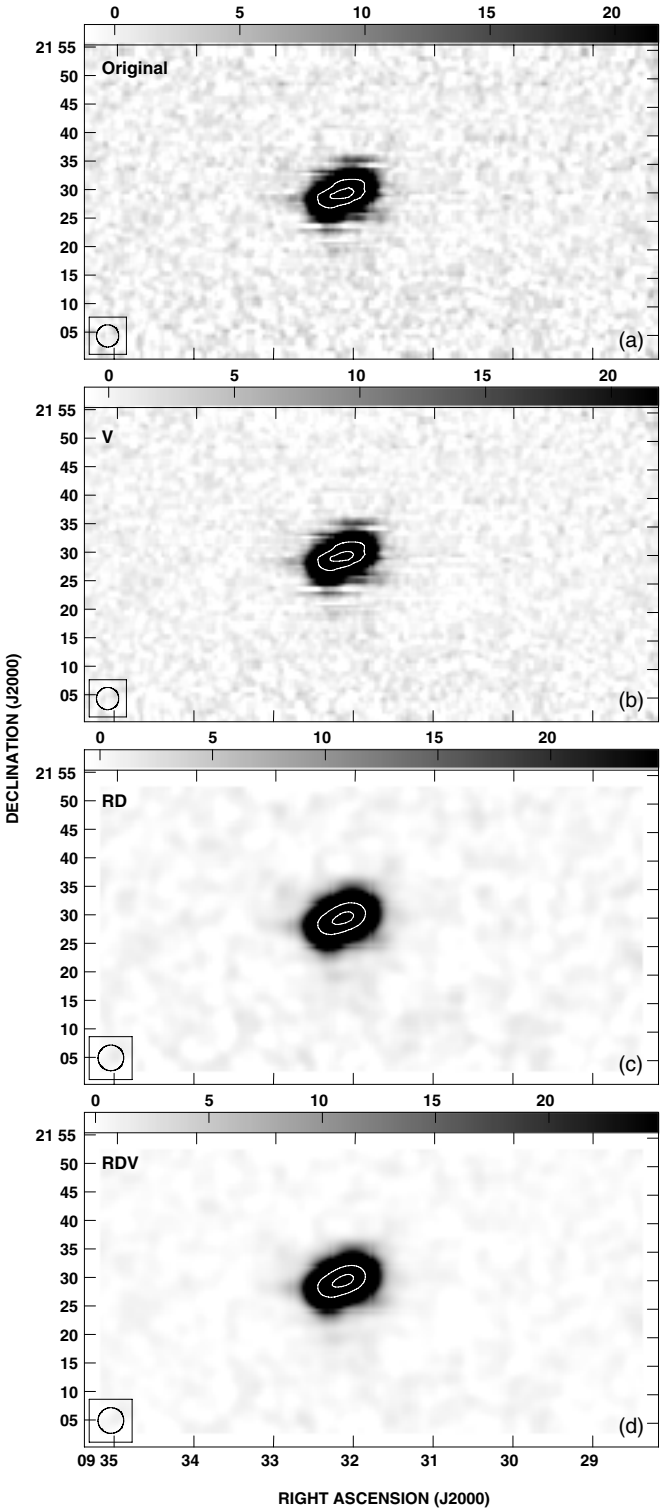

Figure 4. Right ascension–declination plots at $V = 555.0$ km s^{-1}, for the Original cube (a), the V-smoothed cube (b), the RD-smoothed cube (c), and the RDV-smoothed cube (d; see Table 4). Right ascension is indicated at the bottom of the lowest frame. In each case, the grayscale range, marked at the top of each frame, goes from -1σ to 10% of the maximum in the frame, the latter being 216.6 mJy beam^{-1} for (a), 218.0 mJy beam^{-1} for (b), 247.1 mJy beam^{-1} for (c), and 247.5 mJy beam^{-1} for (d). Contours at 50% and 90% of the peak are also shown, as are the beam sizes in each frame.

detection criterion of $\sim 15\sigma 2\delta V = 5\,\mathcal{S}_{\rm lim}$ ($\approx 10^{18}$ cm^{-2} in column density) is likely appropriate in these high-dynamic range regions; that is, the detection limits of Table 4 should be increased by a factor of 5 for regions occupied by NGC 2903 emission itself. We defer the detailed analysis required to determine the outer H I morphology of NGC 2903 to a future paper. We emphasize that these artifacts arise only near bright emission, and thus the sensitivity limits given in Table 4 using $\mathcal{S}_{\rm lim}$ in Equation (1) are appropriate for regions of the data cubes in which we search for companions (see Section 7.2).

Table 5
H I Properties of NGC 2903

Parameter	Value
$\Delta\ V_{50}$ (km s^{-1})[a]	370 ± 2
$\Delta\ V_{20}$ (km s^{-1})[b]	383 ± 2
$V_{\rm sys}$ (km s^{-1})[c]	555 ± 2
$\int S_V\, dV$ (Jy km s^{-1})[d]	255 ± 15
$M_{\rm HI}$ ($M_\odot$)[e]	$(4.8 \pm 0.3) \times 10^9$
$d_{\rm HI}/d_{\rm opt}$[f]	3.2

Notes.
[a]Full width at 50% of the average of the two profile peaks.
[b]As in a but at 20%.
[c]V at the midpoint of ΔV_{20}.
[d]Integral of flux density associated with NGC 2903. The dominant uncertainty is from the baseline flattening; excluding this effect, the uncertainties are of order 1%.
[e]H I mass, from Equation (2) substituting $\int S_V dV$ for $\mathcal{S}_{\rm lim}$.
[f]Ratio of H I to optical major axis diameter. $d_{\rm HI}$ is measured at 10^{18} cm^{-2} and $d_{\rm opt}$ is from Table 2.

7. RESULTS

7.1. Basic Properties of NGC 2903

While a detailed analysis of the H I morphology and kinematics of NGC 2903 is beyond the scope of this paper, we present some of its basic properties here to illustrate the content and quality of our data cubes.

7.1.1. Global Parameters

Figure 6 shows the global profile of NGC 2903, and corresponding global parameters are given in Table 5. The profile shape agrees well with previously published plots (Wong et al. 2006; Hewitt et al. 1983) and our integrated flux density (Table 5) agrees with the result of Braun et al. (2007) to within errors. There is an obvious asymmetry in the galaxy, such that the low-velocity peak (northeast side of galaxy) is higher than the high-velocity peak (southwest side). The integrated flux on the low-velocity side of the galaxy is 13% higher than on the high-velocity side, denoting an intrinsic asymmetry in the H I distribution of that order.

7.1.2. Morphology and Kinematics

We present the integrated intensity and intensity-weighted mean velocity fields, from the RDV-smoothed cubes, in Figure 7. A small, previously unknown H I companion can be seen 24.′8 (64.3 kpc in projection) to the northwest. The eastern companion, UGC 5086, is enveloped in the H I emission from NGC 2903. H I companions will be discussed further in Section 7.2.

We find a very large H I envelope around NGC 2903, even accounting for the Arecibo beam and residual map errors. For comparison, the gray contour in Figure 7(a) shows the outermost significant integrated intensity level (1×10^{19} cm^{-2}) in the archived D-configuration VLA observations (see Section 3),

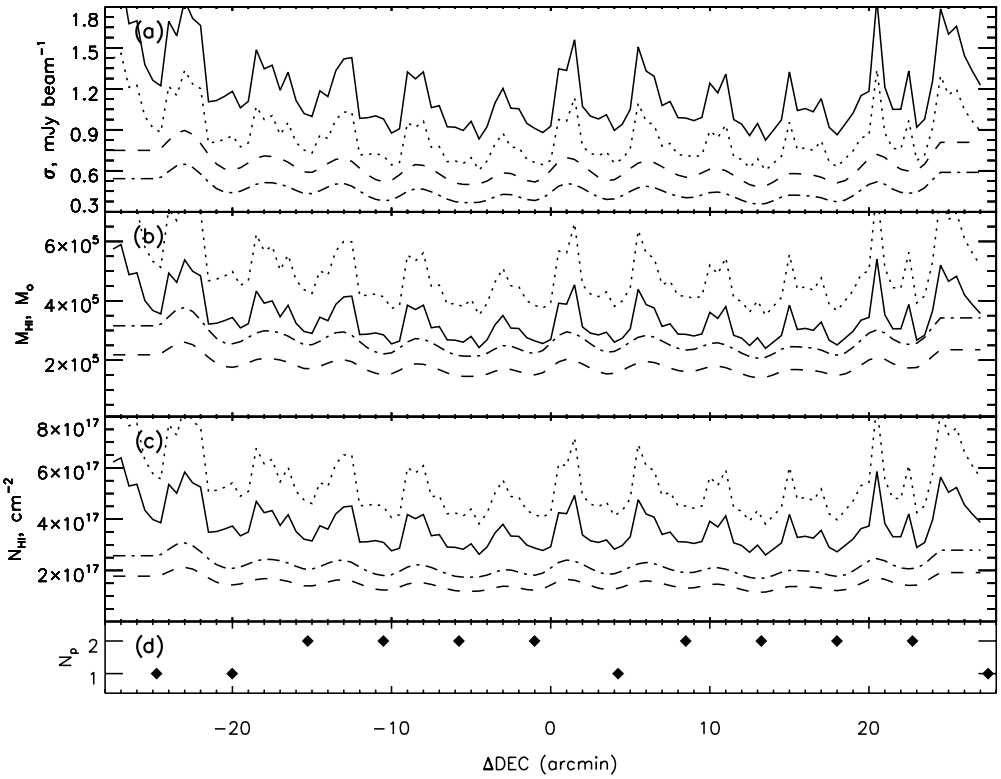

Figure 5. Noise and detection thresholds as a function of decl. Δ DEC is relative to the optical center of NGC 2903 (Table 1). In each panel, the solid curve represents the original cube, the dotted curve represents the V-smoothed cube, the dashed curve represents the RD-smoothed cube, and the dash-dotted curve represents the RDV-smoothed cube (Section 5.3, Table 4). (a) rms noise σ. (b) Minimum detectable H I mass $M_{HI\,lim}$, given by Equation (2). (c) Minimum detectable column density $N_{HI\,lim}$, given by Equation (3). (d) Number of passes (i.e. drifts) N_p as a function of the declination of the central ALFA beam (Beam 0).

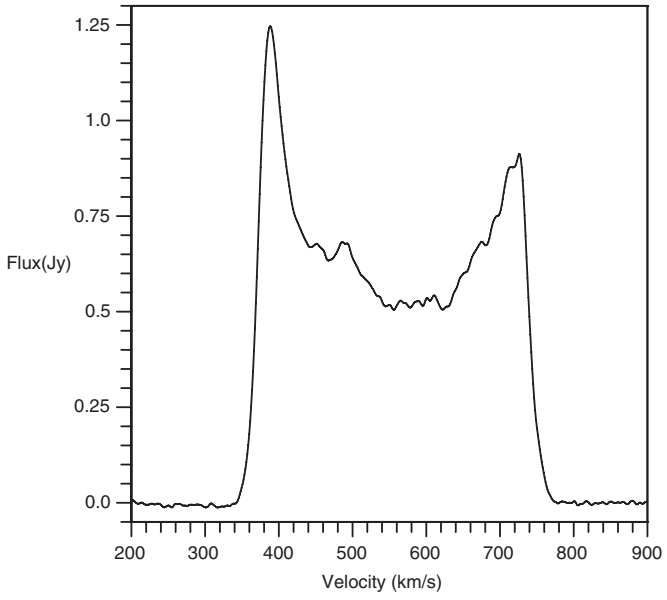

Figure 6. Global profile of NGC 2903. Errors (ignoring any uncertainty in baseline flattening) are typically within 1% except where the profile approaches zero.

smoothed to the same resolution as the Arecibo data in the figure. The major axis diameter at 10^{18} cm^{-2} in our Arecibo data—which should be immune to residual map errors (see Section 6.2) is $d_{HI} = 40.'7$ (105 kpc) after correcting for the beam, nearly twice the value measured from the VLA data. Thus, the H I extent of NGC 2903 is at least 3.2 times its optical diameter (Table 1) and ranks among the largest known (Matthews et al. 2001; del Rio et al. 2004; Spekkens & Giovanelli 2006; Oosterloo et al. 2007; Curran et al. 2008).

The velocity field of NGC 2903 (Figure 7(b)) shows regular rotation, with the northeast side advancing with respect to the center. The contours indicate that the outer H I disk of the galaxy is warped in spite of its apparent isolation. A position–velocity plot along a 270″ wide strip of the major axis is shown in Figure 8. The inner rotation curve of NGC 2903 appears to be regular, but it is strongly biased by beam smearing and not a good indicator of the gravitational potential in these regions. We find no evidence for gas at anomalous velocities at the sensitivity and resolution of our data.

7.2. H I Companions of NGC 2903

7.2.1. The Known Companion, UGC 5086

UGC 5086 is the only previously known companion of NGC 2903 that lies within the surveyed region (see Section 3). This galaxy overlaps the large H I envelope of NGC 2903 in both position and velocity space. Figure 9, which shows a single channel at the systemic velocity of UGC 5086, illustrates this blending. A global profile from a $3' \times 3'$ box centered on UGC 5086 in the RDV-smoothed cubes yields a spectrum (not shown) with a peak of 4.4 mJy at $V = 497$ km s^{-1}, resulting in a measured H I mass of $M_{HI} = 9.0 \times 10^6\ M_\odot$ (Equation (2) substituting the integrated flux of the profile for $\mathcal{S}_{lim}$). While the velocity of the spectral peak agrees with the systemic velocity of UGC 5086 (Table 2), the detected signal could also arise from the envelope of NGC 2903 itself. To help distinguish between signal from UGC 5086 and NGC 2903, we have searched our reduced VLA D-configuration (Section 3) data, which clearly separate the two galaxies spatially. We find no emission from

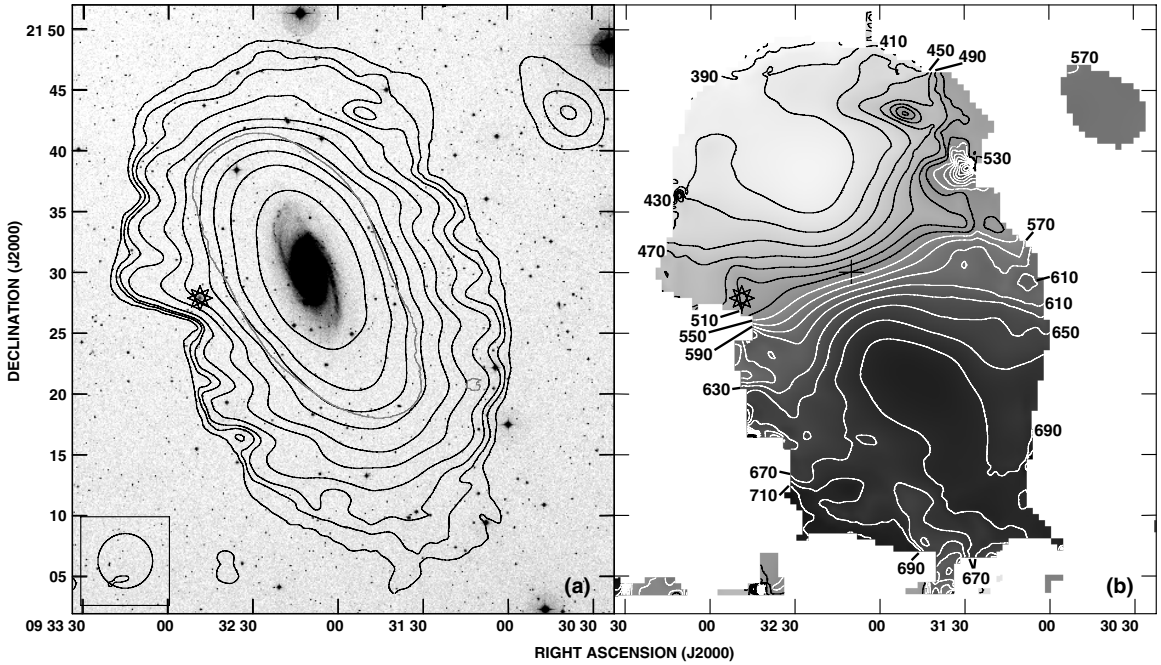

Figure 7. Moment maps of NGC 2903, constructed from the RDV-smoothed cubes. The location of the galaxy, UGC 5086 is marked with a star. Detailed maps of the companion to the northwest of NGC 2903 are in Figure 12. (a) Total intensity H I map over the DSS2 Blue image, the latter shown in an arbitrary grayscale. Contours are at 0.02, 0.06, 0.10, 0.20, 0.50, 1.0, 2.5, 5, 10, and 25 Jy beam^{-1} km s^{-1}. The peak is 68.3 Jy beam^{-1} km s^{-1}. The beam is shown at lower left. A conversion to column density requires a multiplication by 1.52×10^{19} cm^{-2} (Jy beam^{-1} km s^{-1})$^{-1}$. Note that there may be residual map errors near NGC 2903 below $\sim 10^{18}$ cm^{-2}; see Section 6.2. The gray curve shows the outermost significant integrated intensity level (1×10^{19} cm^{-2}) in the archived D-configuration VLA observations (see Section 3), after smoothing the VLA cube to the same spatial resolution as the Arecibo data. (b) Intensity-weighted mean velocity contours over a grayscale from the same image. Contours, in km s^{-1}, are labeled and are spaced 20 km s^{-1} apart. The optical center of the galaxy is marked with a cross.

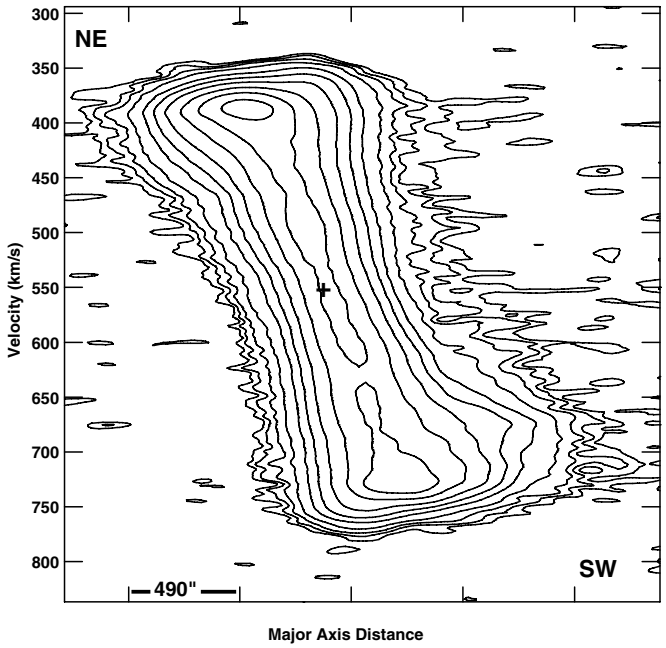

Figure 8. Position–velocity plot along the major axis of NGC 2903, from the RDV-smoothed cube, averaged over a width equivalent to the beam size. The center is marked with a cross. Contours are at 1.0 (2σ), 1.8, 3.0, 6.0, 15, 30, 60, 120, 200, and 300 mJy beam^{-1}. The northeast (NE) and southwest (SW) sides of the galaxy are labeled and tickmarks along the position axis are separated by 490″. Note that there may be residual map errors below $\sim$ 3% near the galaxy; see Section 6.2.

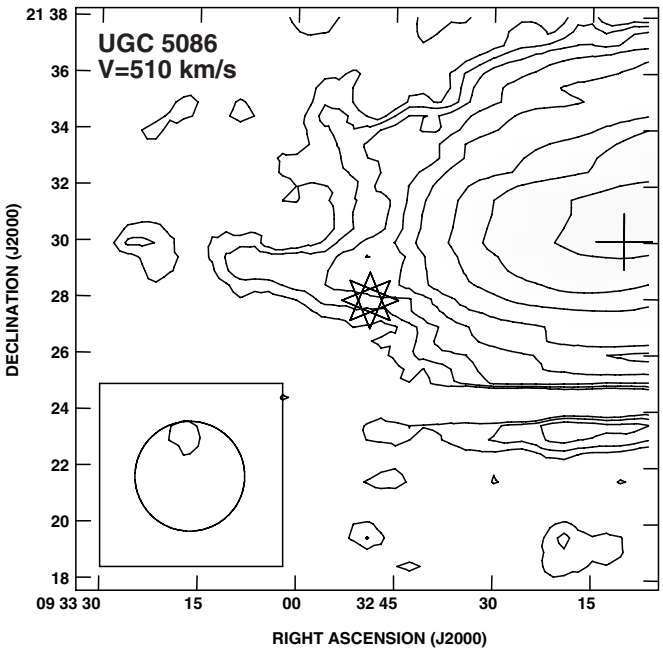

Figure 9. Single channel of the V-smoothed cube centered on the position and velocity (Table 2) of the companion, UGC 5086. The companion is seen within the region of a protrusion to the east of the H I envelope associated with NGC 2903. UGC 5086 is marked with a star and the center of NGC 2903 is marked with a cross to the west. Contours are at 1.6 (2σ), 3.0, 5.0, 10, 20, 50, 100, and 200 mJy beam^{-1}. Note that there may be residual map errors below $\sim$ 3%; see Section 6.2. The beam is shown at lower left.

UGC 5086, and place an upper limit on the H I mass in a single 54″ beam of $M_{\rm HI\,lim} = 5.6 \times 10^5\ M_\odot$ from the VLA data. Thus, our Arecibo detection is primarily from NGC 2903 iself.

UGC 5086 is well resolved in the SDSS Data Release 6 (DR6). Its image appears almost perfectly circular and it has a red color ($B_0 - V_0 = 0.79$, using SDSS magnitudes and applying

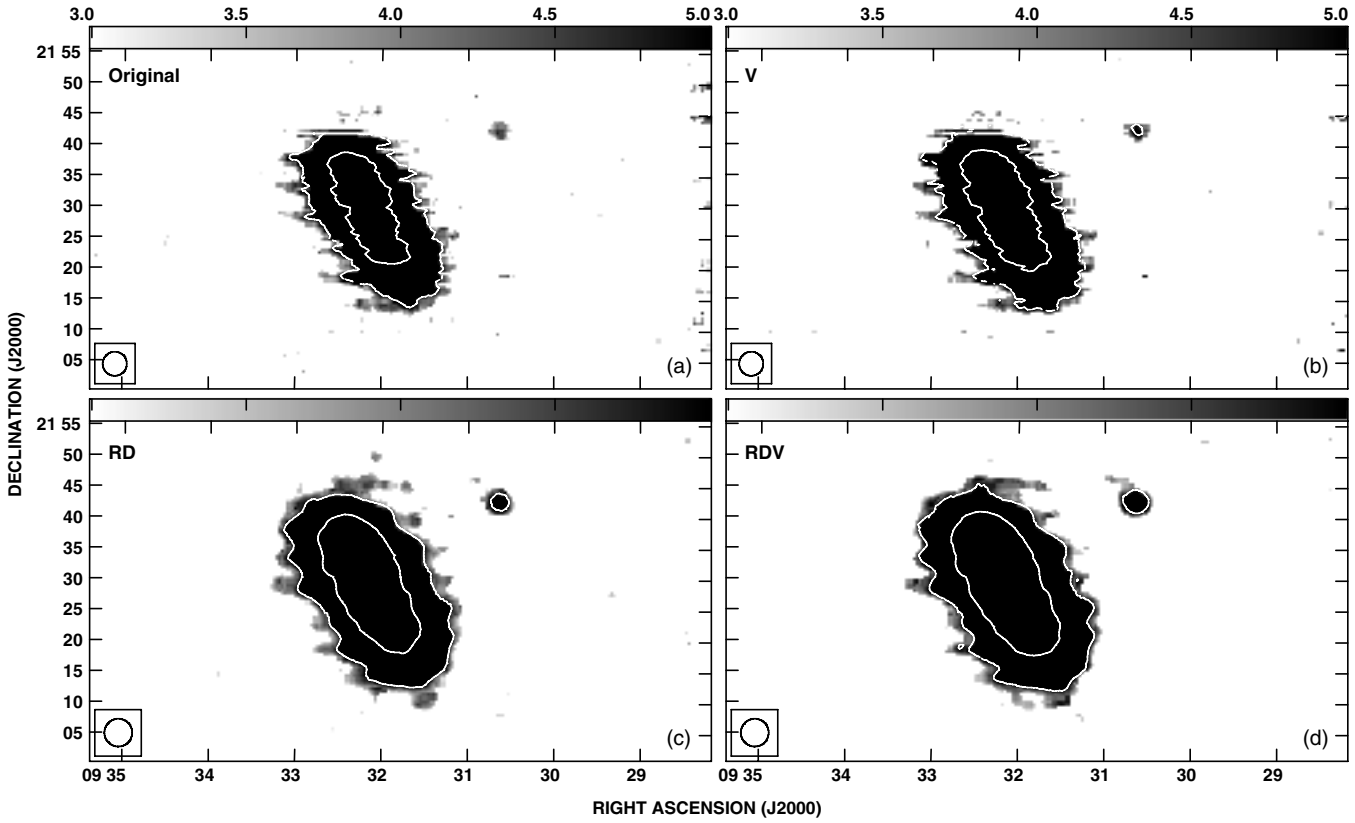

Figure 10. Summed S/N maps for each of the four cubes (labeled at top left in each frame). Only points $\geqslant 3\sigma$ that are detected in $\geqslant 2\delta V$ independent velocity resolution elements, as described in Section 7.2.2, have been included in the maps. Low levels have been emphasized, with a grayscale range ($3\sigma - 5\sigma$) shown at the top, and the 5σ and 50σ contours are also shown. The beam is shown at lower left. Peak levels are 161σ, 216σ, 256σ, and 343σ for (a), (b), (c), and (d), respectively. Note that there may be residual map errors below the 5σ contour in NGC 2903; see Section 6.2.

transformations referenced in Section 7.2.3). Given the absence of H I and known optical parameters, it is likely that UGC 5086 is a dwarf spheroidal galaxy without H I content. We note that near-UV emission can be seen in UGC 5086 also,[31] suggesting the presence of a young stellar population. This is similar to the dwarf spheroidal galaxy, Fornax, which contains both old, intermediate, and young stars (Battaglia et al. 2006).

7.2.2. Search for New Companions

A visual search of the data cubes has revealed a new H I-rich companion to NGC 2903, visible in Figure 7. This companion, which we designate N2903-HI-1, will be discussed further in Section 7.2.3. In order to detect companions in a more quantitative fashion, it is important to account for the variation in map noise, σ, with declination, illustrated in Figure 5(a). To this end, we formed signal-to-noise ratio (S/N) cubes[32] by dividing each datapoint by the σ corresponding to its decl., and searched for emission exceeding $\mathcal{S}_{\rm lim}$ from Equation (1). Specifically, we integrated each S/N cube over all V including only those points that exceed 3σ over at least two adjacent independent velocity resolution elements.[33] The resulting summed maps, which emphasize faint emission, are shown in Figure 10.

Figure 10 confirms that N2903-HI-1 is the only bona fide H I-rich companion to NGC 2903 in our data. While other isolated nonzero pixels are also seen in the various maps, they are clearly random noise peaks. This is corroborated by the lack of correlation between the locations of these pixels in the different maps.

There is a possibility that companions may lie within the spatial region over which NGC 2903 is found, but at anomalous velocities in comparison to NGC 2903. We have searched through this parameter space and find no evidence for such H I clouds (see also the major axis slice of Figure 8).

It is also plausible that our search has missed companions which overlap NGC 2903 in *both* position and velocity space, a possibility raised by the location of UGC 5086 (Section 7.2.1). The H I disk of NGC 2903 occupies an exceedingly small percentage of the total volume surveyed, however, making such a coincidence highly unlikely. Moreover, if a starless H I emission feature exists within the H I position–velocity envelope of NGC 2903, then it becomes moot as to whether such a feature should simply be considered part of NGC 2903 itself.

7.2.3. The New Companion, N2903-HI-1

N2903-HI-1 is separated from NGC 2903 by 24.′8 spatially (64.3 kpc in projection) and by +26 km s^{-1} in velocity (see Tables 1 and 6). Its global profile is shown in Figure 11, and related parameters are given in Table 6. We also show the total intensity map, a position–velocity slice, and the 1st and 2nd moments of the H I distribution in Figure 12. The full velocity resolution cube has been used for the latter two maps since the profile is narrow.

Figure 12(a) illustrates that N2903-HI-1 is elongated north-east to south-west and has a "cometary" or "head-tail" morphology. In spite of the large beam size, the companion is spatially

[31] http://skyview.gsfc.nasa.gov.
[32] The S/N cubes may be download from our Web site.
[33] Our AIPS-compatible routine (xsmc), written for this purpose, is available on our Web site.

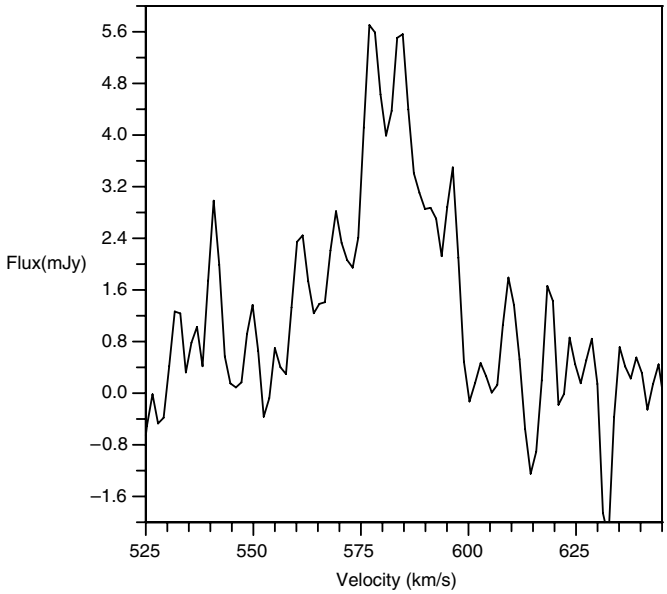

Figure 11. Global profile of the companion, N2903-HI-1, obtained from the RD-smoothed cubes.

resolved in all cubes, hence its radius, R, can be measured. This has been done via a Gaussian fit to the highest spatial resolution data and deconvolving the beam (Table 6).

We do not find convincing evidence of systematic motion in our data, either from the major axis slice (Figure 12(b)), the first moment map (Figure 12(c)), or channel maps (not shown). A rotating disk with an inclination $i > 15^\circ$ would exhibit a gradient across the disk that is greater than the typical velocity dispersion of 6 km s^{-1} in Figure 12(d). Thus, if the H I represents a disk in rotation, we might have expected, given our fine velocity resolution, to have seen some evidence for this. Given the elongated morphology of the H I, it seems more likely that it is being either tidally perturbed or ram pressure stripped via passage through a gaseous medium. Head-tail morphologies are typically seen in the latter case, but because of low spatial resolution, the former cannot be ruled out.

To determine a total dynamical mass, ideally we would want to associate the radius of N2903-HI-1 with some rotational velocity. As we do not know the precise geometry of the system and do not see rotation, this association cannot be made. However, the measured line width and radius should provide us with some measure of the total mass which we now estimate under two assumptions that should encompass the extrema of possibilities (see Westmeier et al. 2005 a for a similar approach).

First, in the event that a rotation might have remained undetected (for example, if the companion represents a rotating galaxy that is near face-on), the dynamical mass, $M_{\rm dyn}$, can be estimated via,

$$M_{\rm dyn}\ \sin^2 i = \frac{R}{G}\left(\frac{\Delta V_{50}}{2}\right)^2, \qquad (4)$$

where ΔV_{50} is the width of the profile in Figure 11 at 50% of the peak (Table 6). ΔV_{50} has been adopted, rather than ΔV_{20}, since the latter is a measurement at a level within the noise. With the assumption of rotation, R may be overestimated if there is a cometary tail that does not take part in the rotation; however, the velocity width, which has been minimized by the choice of ΔV_{50}, has a greater effect. Together with what would be a substantial correction for the unknown inclination, the result for $M_{\rm dyn}$ (Table 6) will be a minimum.

Table 6
Properties of N2903-HI-1

Parameter[a]	Value
R.A. (h m s)[b]	09 30 38
decl. ($^\circ$ $'$ $''$)[b]	21 43 08
$\Delta\ V_{50}$ (km s^{-1})[c]	23.6 ± 5.2
$\Delta\ V_{20}$ (km s^{-1})[d]	40.2 ± 5.2
$V_{\rm sys}$ (km s^{-1})[e]	582 ± 4
$\int S_V\, dV$ (Jy km s^{-1})[f]	0.14 ± 0.02
$M_{\rm HI}$ ($M_\odot$)[g]	$(2.6 \pm 0.3) \times 10^6$
R (arcsec)[h]	90 ± 40
(kpc)	3.9 ± 1.7
$M_{\rm dyn}\ \sin^2$(i) ($M_\odot$)[i]	$(1.3 \pm 1.1) \times 10^8$
$M_{\rm vir}$ ($M_\odot$)[i]	$(4.5 \pm 4.0) \times 10^8$

Notes.
[a]Table 5 provides definitions when not indicated here.
[b]Position of peak of the total intensity map (Figure 12(a)). The uncertainty is $\sim 15''$ (1/2 the cellsize) in RA and $\sim 1'$ (1/4 of the beam) in decl.
[c]Full width at 50% of the profile peak. The error bar encompasses variations between the cubes.
[d]As in b but at 20%.
[e]Average of V at the midpoint of ΔV_{20} and ΔV_{50}.
[f]Uncertainty is dominated by variations between the different cubes and choice of velocity window.
[g]Assuming the distance is the same as NGC 2903.
[h]Radius of N2903-HI-1, from 1/2 of the FWHM found from deconvolved Gaussian fits to the total intensity map.
[i]Dynamical ($M_{\rm dyn}$), and virial ($M_{\rm vir}$) masses, as given by Equations (4) and (5), respectively.

Secondly, for comparative purposes, we assume virial equilibrium for which,

$$M_{\rm vir} = \frac{5\ R\ (\Delta V_{50})^2}{8\ G\ \ln 2}. \qquad (5)$$

Here, we have related the mean-square velocity of the particles, $\langle v^2 \rangle$, to the observed FWHM velocity width, ΔV, according to $\langle v^2 \rangle = 3\,(\Delta V)^2/(8\ \ln 2)$ (Westmeier et al. 2005b).

The results (Table 6) indicate a total mass for N2903-HI-1 which exceeds $10^8\ M_\odot$ by either estimate (Table 6), and we adopt the mean, $3 \times 10^8\ M_\odot$, as a "characteristic" dynamical mass. Although the error bars are substantial, it is nevertheless clear that the H I mass of N2903-HI-1 is only a small fraction of its total mass.

Does N2903-HI-1 have an optical counterpart? Because of the elongated shape of the H I emission, it is possible that an optical galaxy could be displaced with respect to the H I central peak. We have therefore searched the SDSS DR6 database over the original full beam width, (3.′9), centered on the peak position of N2903-HI-1 (Table 6). There are 207 cataloged sources in this area, each with photometric, rather than spectroscopic redshifts. Given that the dispersion between spectroscopic and photometric redshifts is of order ≈ 0.06 (Csabai et al. 2003) at low redshift, we have identified all galaxies with redshifts less than 0.06 over this spatial region. The result gives 34 galaxies, all of which are plotted in Figure 12(a). Stellar masses have been calculated for each of these galaxies according to the formalism of Bell et al. (2005), assuming a Kroupa (2001) Initial Mass Function (IMF), and assuming that they are at the distance of NGC 2903. If a modified Salpeter IMF is used instead (Bell et al. 2003), the stellar mass increases by only a factor of 1.4.

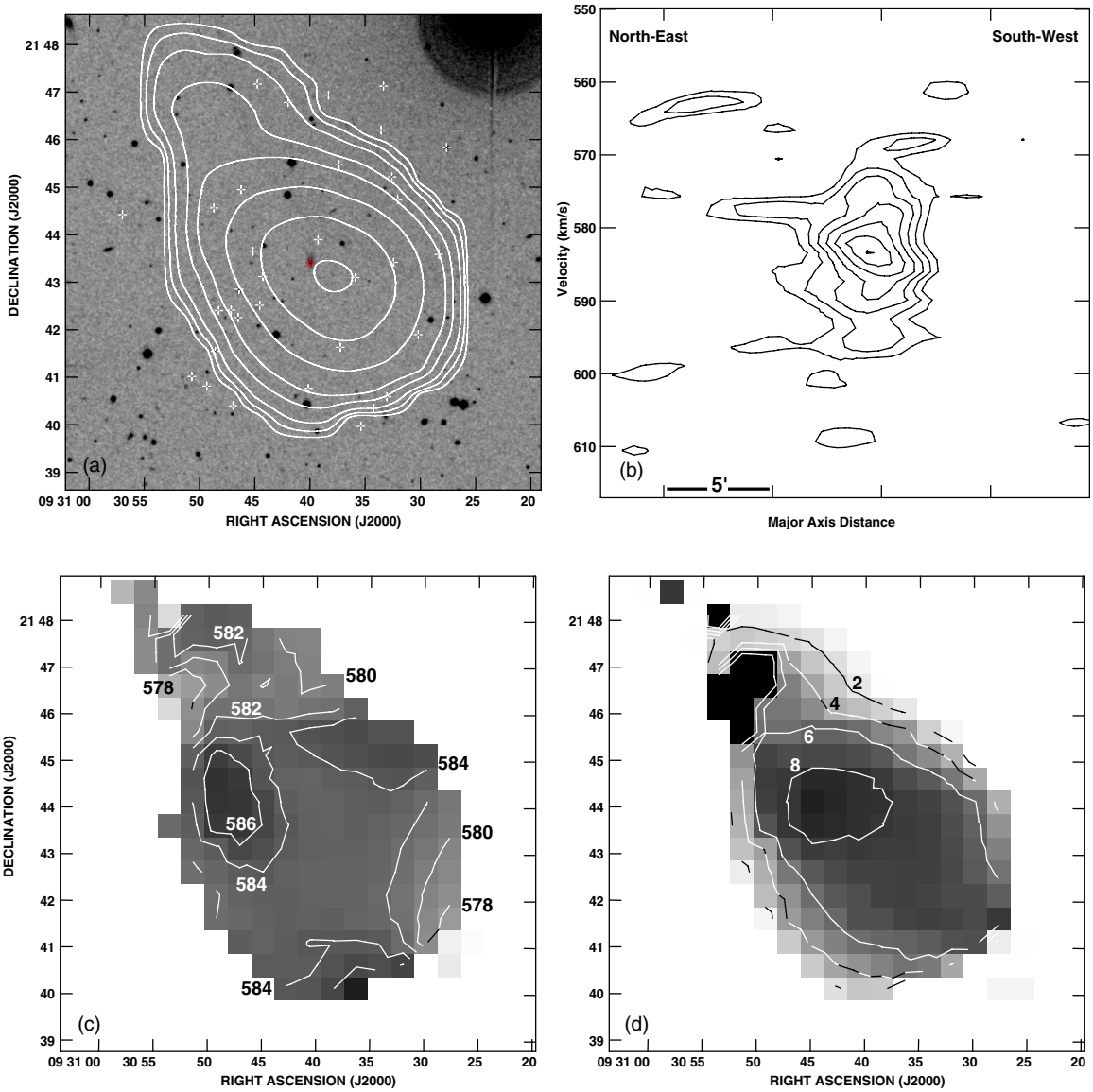

Figure 12. H I maps of the companion, N2903-HI-1. (a) Total intensity map, from the RDV-smoothed cubes integrated over 540–617 km s^{-1}, superimposed on the DSS2 Blue image. Contours are at 2, 5, 10.0, 20, 30, 50, 75, and 100 Jy $beam^{-1}$ m s^{-1}. The column density conversion is 1.52×10^{19} cm^{-2} (Jy $beam^{-1}$ km $s^{-1})^{-1}$. Crosses mark the locations of all low redshift optical galaxies in the vicinity (Section 7.2.3) and the red cross indicates the most probable companion (Table 7). (b) Position–velocity slice from the RDV-smoothed cubes, averaged over a 4′ wide swath at a position angle of 45°. Contours are at 1.0, 1.5, 2.0, 2.5, 3.0, 3.5, and 3.9 mJy $beam^{-1}$. The angular distance scale is marked at the bottom. (c) Intensity-weighted mean velocity, from the RD-smoothed cubes, using the same velocity range as in (a). Contours are at 578, 580, 582, and 584 km s^{-1} and the grayscale ranges from 567 to 593 km s^{-1}. (d) Intensity-weighted velocity dispersion, from the RD-smoothed cubes, with contours at 2, 4, 6, and 8 km s^{-1} and using the same velocity range as in (a). The grayscale ranges from 0.6 to 10 km s^{-1}. The black pixels to the northeast included noise and are spurious.

(A color version of this figure is available in the online journal.)

The galaxy, SDSS J093039.96+214324.7 (see Table 7), which is marked in red in Figure 12(a), is the most likely optical counterpart for several reasons. First, the position of this galaxy agrees with the peak of N2903-HI-1 within errors (Tables 6 and 7). It is also significantly brighter (by at least 2.9 mag in *g*), larger and has more stellar mass[34] than other candidates in the field. A 2nd Digital Sky Survey (DSS2) image of this galaxy is shown in Figure 13, and reveals a galaxy that is elongated roughly northen–south, similar to the H I morphology of N2903-HI-1 (see Figure 12) but at a different position angle. Assuming that J093039.96+214324.7 is at the distance of NGC 2903, we list its properties Table 7.

At the distance of NGC 2903, the properties of J093039.96+214324.7 indicate that it is a low luminosity dwarf galaxy with a linear diameter of approximately 1 kpc. If this galaxy is the optical counterpart of N2903-HI-1, then its stellar mass rivals its H I mass but is at least two orders of magnitude less than its total mass, leading to the conclusion that the system is dark matter dominated. (If J093039.96+214324.7 is not the optical counterpart, the same conclusion is reached.) The H I envelope of N2903-HI-1 extends to ∼ 8 optical radii. Comparing J093039.96+214324.7 to known Local Group dwarfs (Mateo 1998) or faint irregular galaxies (Begum et al. 2008), we find

[34] The stellar mass of the second most massive galaxy is only 37% lower, but it is separated from the peak of N2903-HI-1 by 3.9 arcmin.

Table 7
Properties of J093039.96+214324.7

Parameter	Value
2a × 2b (″ × ″)[a]	22 × 12
(pc × pc)[a]	950 × 518
cz (km s^{-1})[b]	200
u, g, r (mag)[c]	18.71, 18.14, 18.00
B_0, V_0 (mag)[d]	18.28, 17.98
M_B, M_V (mag)[e]	−11.47, −11.77
$M_\star$ ($M_\odot$)[f]	1.8×10^6
$M_{\rm HI}/L_B$ ($M_\odot/L_\odot$)[g]	0.43

Notes.
[a]Major × minor axis dimensions from the 2 σ contour of Figure 13.
[b]Photometric redshift from the SDSS DR6.
[c]Magnitudes in SDSS u, g, and r bands.
[d]B and V magnitudes from the transformation of Lupton (2005), corrected for Galactic extinction (Schlegel et al. 1998).
[e]Absolute B and V magnitudes.
[f]Stellar mass, derived from $B_0 - V_0$ and M_V assuming a Kroupa IMF (Bell et al. 2005).
[g]Ratio of H I mass (Table 6) to blue luminosity, the latter from M_B, with a Solar B-band magnitude of 5.48.

that its color, ($B_0 - V_0 = 0.31$), radius, line width, total mass, and H I mass to blue light ratio ($M_{\rm HI}/L_B$) fall within observed ranges for these other known systems. Although its recessional velocity differs from that of N2903-HI-1, the difference falls within typical errors for photometric redshifts of nearby systems (Csabai et al. 2003). Thus, the position and properties of J093039.96+214324.7, in comparison to the other galaxies in the region, all suggest that this galaxy is the likely optical counterpart of N2903-HI-1. A spectroscopic redshift for this system would decide the matter.

We note that the H I mass of N2903-HI-1 also falls within the range of Galactic HVCs for which there are distance constraints (Putman et al. 2002, Thom et al. 2008; Wakker et al. 2007; Wakker et al. 2008) and at the upper end of the H I mass distribution found for the HVCs around M 31 and M 33 (Thilker et al. 2004; Westmeier et al. 2005a, Westmeier et al. 2007). However, its separation from NGC 2903 (64 kpc in projection) is larger than the population of HVCs around the MW (less than 10–15 kpc typically; Thom et al. 2008) or M 31 (within 50 kpc; Westmeier et al. 2007). In combination with the evidence for an optical counterpart, we consider this interpretation for N2903-HI-1 to be less likely.

8. DISCUSSION

In our targeted sensitive H I survey of the isolated MW analog, NGC 2903, we have discovered one new companion, the H I object, N2903-HI-1, which is dark matter dominated (Table 6) and is likely associated with the optical dwarf galaxy, SDSS J093039.96+214324.7. New discoveries of dwarf satellites of the MW from the SDSS place their typical total masses in the $10^{6-7} M_\odot$ range (Simon & Geha 2007) which is lower than the total mass of $> 10^8\ M_\odot$ (Table 6) found for N2903-HI-1. Combining data from previously known MW companions, the new SDSS companions, and those of M 31, most satellites which still contain detectable H I lie beyond 300 kpc radius, the implication being that H I has been stripped in closer systems (Putman et al. 2008; Grcevich & Putman 2009), although notable exceptions also occur (e.g., the Large and Small Magellanic Clouds). N2903-HI-1, at a projected distance of 64 kpc from NGC 2903, would have to lie at least 293 kpc in front of or behind NGC 2903 to be at a true separation > 300 kpc. Although this is possible, it is more likely that the companion is closer to NGC 2903, yet has retained its H I–a result that may be related to its high dynamical mass in comparison to most MW systems within the same radius. Thus, if ram pressure stripping is occurring, as suggested by the head-tail morphology of N2903-HI-1, the process may be slower because of its high dynamical mass.

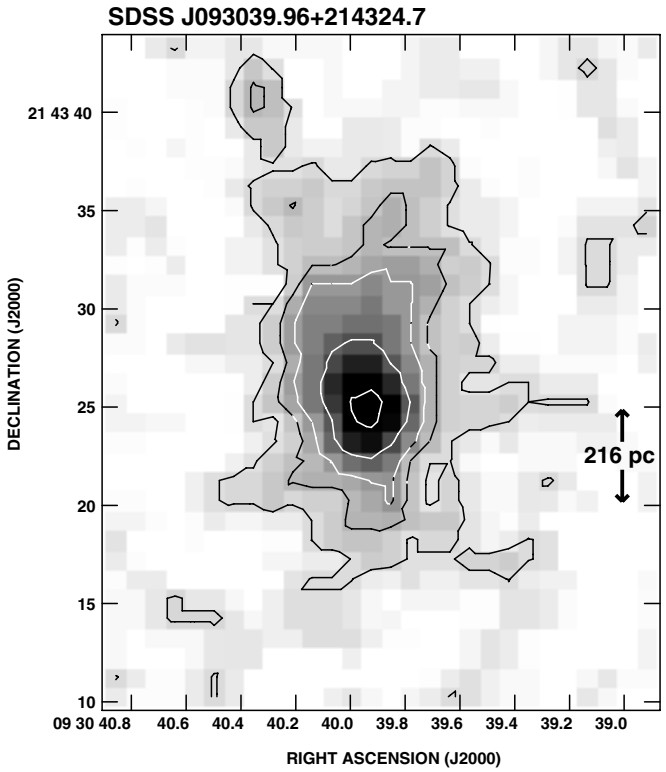

Figure 13. Galaxy, SDSS J093039.96+214324.7, which is the most likely optical counterpart to NGC 2903-HI-1. The image is from the DSS2 Blue image and contours are shown in arbitrary units, with the first contour set at the 2σ level. The scale, for a distance equal to that of NGC 2903, is shown at right.

Although the true separation and space velocity of N2903-HI-1 are not known, we can at least adopt the projected separation and radial velocity offset from NGC 2903 to determine whether the above speculation is feasible. Approximating N2903-HI-1 as a sphere, its average ISM H I density, from the values of Table 6, is $n_{\rm ISM} \approx 4 \times 10^{-4}$ cm^{-3}. A simple condition for stripping is,

$$n_{\rm halo}\, V_{\rm rel}^2 \;>\; n_{\rm ISM}\, G\, {\rm M_{tot}}/R, \qquad (6)$$

where $\rm M_{tot}$ is the total mass of N2903-HI-1 and R is its radius. Using $M_{\rm tot} = 3 \times 10^8\ M_\odot$, $V_{\rm rel} = 26$ km s^{-1} (Section 7.2.3) and R from Table 6, and solving for halo density, we find $n_{\rm halo} = 2 \times 10^{-4}$ cm^{-3}. This value is within the expected range of halo densities for the MW at the projected distance of N2903-HI-1 (64 kpc; Grcevich & Putman 2009). If the relative velocity is larger, stripping will be more effective, and if the true separation is larger, stripping will be less effective since the halo density will be lower. Nevertheless, this estimate indicates that N2903-HI-1 could indeed be undergoing ram pressure stripping under the assumption that the halo of NGC 2903 resembles the MW. The stripping timescale depends on the difference between the two sides of Equation (6) which is not known. However, since the magnitudes of the ram pressure and the internal energy

density of the companion are similar, the stripping timescale may be long, consistent with the observation of detectable H I in the companion.[35]

It is now interesting to ask how many Local Group dwarf galaxies would have been detected, if they were distributed around NGC 2903 similarly to the MW. The result is dependent on both their distribution and H I content. Seventeen Local Group dwarf galaxies listed in Mateo (1998) had sufficient data (distances and H I data) that we could apply our $3\sigma 2\delta V$ detection criterion (Section 6.1) to them. The result is that we could have detected seven of them (41%) in terms of sensitivity limits. However, these seven galaxies lie at radii between 490 kpc and 1.6 Mpc, in comparison to the effective projected radius of $R_{\rm eff} = 110$ kpc (for a circularized field) of our survey. Since our survey probes a volume that is only 0.7% of the volume extending to 1.6 Mpc, it is unlikely that any of these seven galaxies would have fallen within our field of view. Although Mateo does not list H I data for the Large and Small Magellanic Clouds (LMC and SMC, respectively) it is clear, however, that we would have detected these systems. Of the 20 new SDSS dwarf Local Group galaxies listed in Simon & Geha (2007), only one (the dwarf irregular, Leo T) has H I content (Ryan-Weber et al. 2008), the remainder being dwarf spheroidals or falling within parameter space intermediate between dwarf spheroidals and globular clusters. Leo T would be marginally detectable in our survey but, at a distance of 420 kpc (Irwin et al. 2007), would also likely lie outside our field of view. In spite of our large survey region, therefore, we are still only probing the inner region of a possible dwarf galaxy population, were it distributed like our own.

As for HVCs, the HVC population around the MW is not easily translated to NGC 2903 since HVC distances (and therefore H I masses) are not well known. Also, H I column densities which are known (typically 10^{19} cm^{-2}; Stanimirović et al. 2006; Putman et al. 2002), will be diluted by large unknown beam filling factors at the distance of NGC 2903 ($234'' = 10$ kpc). We can say, however, that the MW's HVC Complex C, with a mass of $4.9 \times 10^6\ M_\odot$ at a distance of 10 kpc from the Sun (Thom et al. 2008), should have been detected, provided it were separated in velocity from the bulk of the H I in NGC 2903 itself. Given the inclination of NGC 2903 and the nature of HVCs, we expect this criterion to have been met. Thus, NGC 2903 lacks such an HVC complex. Indeed, given that our search velocity range was over 1000 km s^{-1} (Table 4) and that the median velocity FWHM of MW HVCs (36 km s^{-1}; Putman et al. 2002) corresponds to 28 velocity channels in our data, it is surprising that no clear HVC detections have been made. Either NGC 2903 lacks HVCs, possibly due the fact that NGC 2903 is isolated, or its HVCs are of very low mass.

No dark starless companions have been detected around NGC 2903. This result is consistent with the ALFALFA survey results which indicate that all extragalactic H I objects can be identified with an optical counterpart (Saintonge et al. 2008). The discovery of one new H I rich dwarf companion now places the total number of companions within our surveyed field ($R_{\rm eff} = 110$ kpc) at two: the H I companion, N2903-HI-1, likely associated with a dwarf galaxy, J093039.96+214324.7, with a dynamical mass $\sim 3 \times 10^8 M_\odot$ (mean of values in Table 6) and UGC 5806, which is likely a dwarf spheroidal galaxy (Section 7.2.1). Using the SDSS data for the latter galaxy and the same transformations as described in Section 7.2.3, the stellar mass of UGC 5806 is $M_\star = 4.7 \times 10^7\ M_\odot$. Gilmore et al. (2007) have shown that mass-to-(V-band) light ratios, M/L_V, for dwarf spheroidal galaxies in the Local Group range from ≈ 4 to 600, with more luminous galaxies having systematically lower values of M/L_V. The absolute magnitude of UGC 5086 is $M_V = -13.7$ which is closest to Fornax, amongst Local Group dwarfs. If UGC 5086 has similar properties, then $3 \leqslant M/L_V \leqslant 20$, implying that $1.0 \times 10^8 \leqslant M/M_\odot \leqslant 5.2 \times 10^8$. Adopting the mid-point of this range gives an estimate of $\approx 3 \times 10^8\ M_\odot$ for the total mass of UGC 5086.

How many dark-matter clumps of total mass $M_{\rm tot} \gtrsim 3 \times 10^8\ M_\odot$ are expected from ΛCDM predictions? Since NGC 2903 has a total mass that is similar to the MW (Section 3), we can use the Via Lactea simulations of subhalo clumps from Diemand et al. (2007a) for comparison. The fraction of all halo mass that is present in substructure within a *projected* radius of 110 kpc (their Figure 7) is $f = 0.02$. With an adopted total halo mass of $1.77 \times 10^{12} M_\odot$, this yields a total mass in halo substructure of $M_{\rm hs} = 3.54 \times 10^{10}\ M_\odot$ for the projected radius. Over the substructure mass range of $4.6 \times 10^6 \leqslant M_{\rm sub}/M_\odot \leqslant 1 \times 10^{10}$, the number of clumps per unit mass range is given by $dN/dM_{\rm sub} = K/(M_{\rm sub})^2$, where K is a constant. Since the slope does not change with radius, we can compute K from $M_{\rm hs} = \int K/(M_{\rm sub})^2\, M_{\rm sub}\, dM_{\rm sub}$, finding $K = 4.6 \times 10^9 M_\odot$. Finally, we compute the expected number of clumps with masses greater than $M_{\rm sub}$ from $N(> M_{\rm sub}) = K/M_{\rm sub}$. For $M_{\rm sub} = 3 \times 10^8\ M_\odot$, this yields 15 clumps in comparison to the two observed. If the dynamical mass of N2903-HI-1 is higher than $3 \times 10^8\ M_\odot$ (for example, if it is rotating and nearly face-on), then the discrepancy reduces. However, its mass would have to be as high as $\sim 5 \times 10^9 M_\odot$ for there to be agreement with the theoretical expectation. Such a high value would require N2903-HI-1 to represent a rotating system in a special geometry with an inclination less than 10° (Section 7.2.3). Again, although this possibility cannot be ruled out completely, it is quite unlikely. Thus, it would appear that there is a discrepancy between the expected number of companions and the number observed.

Since we have a detection threshold that is lower still than the value of the detected companion, we can also ask how many dark-matter clumps would we expect to see, were they H I rich. For example, our lowest H I detection threshold is $2 \times 10^5\ M_\odot$ (Table 4). If $M_{\rm tot}/M_{\rm HI} \approx 100$ for a dwarf galaxy in the field (equivalent to the N2903-HI-1 value), then we could have detected companions of total mass as low as $2 \times 10^7\ M_\odot$ via their H I. Therefore, within our field of view, using the above relation, we should have detected 230 galaxies as opposed to that observed. This is strongly discordant with ΛCDM. The conclusion is that, if this many dark-matter clumps exist in the region, then they are clearly not H I rich, i.e. they contain no H I or they contain H I at a level lower than 1%.

9. CONCLUSIONS

Using the Arecibo telescope with the ALFA receiver, we have mapped NGC 2903 and its environment with very high sensitivity and coverage. Our lowest point source detection limit is $2 \times 10^5\ M_\odot$ and almost 40 thousand square kpc of sky has been fully covered. The Arecibo ALFA beams have been carefully characterized as a function of azimuth, allowing us to clean each beam as a function of azimuth from the H I datacube. With a velocity coverage of 1035 km s^{-1} and fine velocity resolution (2.6 km s^{-1}), our combination of observing parameters makes this survey unique and among the most sensitive and complete

[35] If ram pressure *did* strongly dominate, then the stripping timescale would be minimized, i.e. $t_{\rm min} \approx 2R/V_{\rm rel} = 3 \times 10^8$ yr.

of a nearby galaxy. Although details of NGC 2903, itself, are left to future work, our results show that the H I envelope around NGC 2903 is much larger than previously known, extending to at least three times the optical galaxy diameter.

The fact that we have targeted an apparently isolated, noninteracting galaxy to a very low-sensitivity limit has clearly been an advantage in the search for H I companions. The discovery of only one isolated H I companion, N2903-HI-1, which appears to have a small optical counterpart, is a significant result. The optical companion is likely a dwarf galaxy with a stellar mass approximately equal to its H I mass with the H I in a broad envelope, approximately eight times larger, around it. The best estimate of its dynamical mass is 3×10^8 $M_\odot$. We have no convincing HVC detections.

In the field surveyed, there are now two known companion galaxies, our new discovery as well as what is likely a dwarf spheroidal galaxy, UGC 5086, the latter with a total mass likely comparable to N2903-HI-1. In this region, ΛCDM scenarios (specifically, the Via Lactea model) predict 15 companions for a MW-type galaxy, with masses greater than 3×10^8 $M_\odot$. Given our H I detection limits, however, *if* companions to NGC 2903 contained H I at the 1% level in comparison to their total masses, then we should have detected 230 of them. If these clumps are present as predicted, they do not contain appreciable H I. They may be starless dark clumps or very low luminosity dark-matter dominated dwarf spheroidals.

We are grateful to students K. Marble of Queen's University and I. Bah, A. Altaf, and J. Goldstein of Lafayette College for their assistance with the data reductions. Many thanks also to P. Perillat and the Arecibo staff for their knowledge and assistance. J.A.I. gratefully acknowledges a grant from the Natural Sciences and Engineering Research Council of Canada. G.L.H. gratefully acknowledges grants from the Lafayette College Academic Research Committee. This research has made use of the NASA/IPAC Extragalactic Database (NED) which is operated by the Jet Propulsion Laboratory, California Institute of Technology, under contract with the National Aeronautics and Space Administration. Funding for the SDSS and SDSS-II has been provided by the Alfred P. Sloan Foundation, the Participating Institutions, the NSF, the U.S. Department of Energy, the National Aeronautics and Space Administration, the Japanese Monbukagakusho, the Max Planck Society, and the Higher Education Funding Council for England. The SDSS Web site is http://www.sdss.org/.

Facilities: Arecibo.

REFERENCES

Auld, R., et al. 2006, MNRAS, 371, 1617
Avila Reese, V., et al. 2001, ApJ, 559, 516
Barkana, R., & Loeb, A. 1999, ApJ, 523, 54
Barnes, D. G., & de Blok, W. J. G. 2004, MNRAS, 351, 333
Barnes, D. G., et al. 2001, MNRAS, 322, 486
Battaglia, G., et al. 2006, A&A, 459, 423
Begeman, K. 1987, PhD Thesis, Rijksuniversiteit te Groningen
Begeman, K. G., Broeils, A. H., & Sanders, R. H. 1991, MNRAS, 249, 523
Begum, A., et al. 2008, MNRAS, 386, 1667
Bekki, K., Koribalski, B. S., Ryder, S. D., & Couch, W. J. 2005, MNRAS, 357, L21
Bell, E. F., McIntosh, D. H., Katz, N., & Weinberg, M. D. 2003, ApJS, 149, 289
Bell, E. F., et al. 2005, ApJ, 625, 23
Benson, A. J., Frenk, C. S., Lacey, C. G., Baugh, C. M., & Cole, S. 2002, MNRAS, 333, 177
Braun, R., Oosterloo, T. A., Morganti, R., Klein, U., & Beck, R. 2007, A&A, 461, 455
Briggs, F. H. 2004, in IAU Symp. 217, Recycling Intergalactic and Interstellar Matter, ed. P. A. Duc, J. Braine, & E. Brinks (San Francisco, CA: ASP), 26
Buie, M. 2008, http://www.lowell.edu/users/buie/idl/idl.html
Cornwell, T., Braun, R., & Briggs, D. S. 1999, Synth. Imaging in Radio Astron. II, 180, 151
Csabai, I., et al. 2003, AJ, 125, 580
Curran, S. J., Koribalski, B. S., & Bains, I. 2008, MNRAS, 389, 63
de Blok, W. J. G., Zwaan, M., Dijkstra, M., Briggs, F. H., & Freeman, K. C. 2002, A&A, 382, 43
del Río, M. S., Brinks, E., & Cepa, J. 2004, AJ, 128, 89
Diehl, R., et al. 2006, Nature, 439, 45
Diemand, J., Kuhlen, M., & Madau, P. 2007a, ApJ, 657, 262
Diemand, J., Kuhlen, M., & Madau, P. 2007b, ApJ, 667, 859
Drozdovsky, I. O., & Karachentsev, I. D. 2000, A&AS, 142, 425
Gilmore, G., et al. 2007, ApJ, 663, 948
Giovanelli, R., et al. 2005a, AJ, 130, 2598
Giovanelli, R., et al. 2005b, AJ, 130, 2613
Gnedin, N. Y., Kravtsov, A. V., & Chen, H.-W. 2008, ApJ, 672, 765
Grcevich, J., & Putman, M. E. 2009, arXiv:0901.4975
Haiman, Z., Rees, M. J., & Loeb, A. ApJ, , 476, 458
Haynes, M. P., van Zee, L., Hogg, D. E., Roberts, M. S., & Maddalena, R. J. 1998, AJ, 115, 62
Hewitt, J. N., Haynes, M. P., & Giovanelli, R. 1983, AJ, 88, 272
Heymans, C., et al. 2008, MNRAS, arXiv:0801.1156v1
Hirashita, H., Takeuchi, T. T., & Tamura, N. 1998, ApJ, 504, L83
Irwin, M. J., et al. 2007, ApJ, 656, L13
Jackson, J. M., et al. 1991, ApJ, 375, 105
Karachentseva, V. E. 1973, The Catalogue of Isolated Galaxies, Astrof. Issledovanija Byu. Spec. Ast. Obs., 8, 3
Kauffmann, G., White, S. D. M., & Guiderdoni, B. 1993, MNRAS, 264, 201
Kennicutt, R. C., Jr. 1998, ApJ, 498, 541
Kilborn, V. A., Forbes, D. A., Koribalski, B. S., Brough, S., & Kern, K. 2006, MNRAS, 371, 739
Klypin, A., Gottlöber, S., Kravtsov, A. V., & Khokhlov, A. M. 1999, ApJ, 522, 82
Koposov, S., et al. 2008, ApJ, 686, 279
Koribalski, B. S., et al. 2004, AJ, 128, 16
Kovac, K., Oosterloo, T. A., & van der Hulst, J. M. 2005, in Proc. IAU Coll. 198, Near-Field Cosmology with Dwarf Elliptical Galaxies, ed. H. Jerjen & B. Binggeli (Cambridge: Cambridge Univ. Press), 351
Kravtsov, A. V., Gnedin, O. Y., & Klypen, A. A. 2004, ApJ, 609, 482
Kroupa, P. 2001, MNRAS, 322, 231
Linder, S. M., et al. 2004, MNRAS, 353, 201
Lupton, R. 2005, http://www.sdss.org/dr6/algorithms/sdssUBVRITransform.html
Martini, P., Regan, M. W., Mulchaey, J. S., & Pogge, R. W. 2003, ApJS, 146, 353
Mateo, M. L. 1998, ARA&A, 36, 435
Matthews, L. D., van Driel, W., & Monnier-Ragaigne, D. 2008, A&A, 365, 1
Mayer, L., et al. 2001a, ApJ, 547, L123
Mayer, L., et al. 2001b, ApJ, 559, 754
Meyer, M. J., et al. 2004, MNRAS, 350, 1195
Minchin, R. F., et al. 2003, MNRAS, 346, 787
Moore, B., et al. 1999, ApJ, 524, L19
Oosterloo, T. A., et al. 2007, A&A, 465, 787
Pérez-Ramírez, D., Knapen, J. H., Peletier, R. F., Laine, S., Doyon, R., & Nadeau, D. 2000, MNRAS, 317, 234
Pisano, D. J., & Wilcots, E. M. 1999, AJ, 117, 2168
Pisano, D. J., & Wilcots, E. M. 2003, ApJ, 584, 228
Pisano, D. J., et al. 2004, ApJ, 610, L17
Pisano, D. J., et al. 2007, ApJ, 662, 959
Putman, M. E., Grcevich, J., & Peek, J. E. G. 2008, ASP Conf. Ser. 396, Formation and Evolution of Galaxy Disks, ed. J. G. Funes & E. M. Corsini (San Francisco, CA: ASP), 233
Putman, M. E., et al. 2002, AJ, 123, 873
Regan, M. W., Sheth, K., & Vogel, S. N. 1999, ApJ, 526, 97
Ryan-Weber, E. V., et al. 2008, MNRAS, 384, 535
Ryder, S. D., et al. 2001, ApJ, 555, 232
Saintonge, A., et al. 2008, AJ, 135, 588
Sanders, D. B., Mazzarella, J. M., Kim, D.-C., Surace, J. A., & Soifer, B. T. 2003, AJ, 126, 1607
Schlegel, D. J., Finkbeiner, D. P., & Davis, M. 1998, ApJ, 500, 525
Shaviv, N. J., & Dekel, A. 2003, arXiv:astro-ph/0305527
Simon, J. D., & Geha, M. 2007, ApJ, 670, 313
Spekkens, K., & Giovanelli, R. 2006, AJ, 132, 1426
Stanimirović, S., et al. 2006, ApJ, 653, 1210

Stoehr, F., White, S. D. M., Tormen, G., & Springel, V. 2002, MNRAS, 335, L84
Taylor, E. N., & Webster, R. L. 2005, ApJ, 634, 1067
Thilker, D. A., et al. 2004, ApJ, 601, L39
Thom, C., et al. 2008, ApJ, 684, 364
Tschöke, D., Hensler, G., & Junkes, N. 2003, A&A, 411, 41
Verley, S., et al. 2007, A&A, 472, 121
Wakker, B. P., et al. 2007, ApJ, 670, L113
Wakker, B. P., et al. 2008, ApJ, 672, 298
Walter, F., et al. 2008, AJ, 136, 2563
Westmeier, T., Braun, R., & Thilker, D. 2005a, A&A, 436, 101
Westmeier, T., Braun, R., Brüns, C., Kerp, J., & Thilker, D. A. 2007, New Astron. Rev., 51, 108
Westmeier, T., Brüns, C., & Kerp, J. 2005b, A&A, 432, 937
Wong, O. I., et al. 2006, MNRAS, 371, 1855
Xue, X.-X., et al. 2008, ApJ, 684, 1143
York, D. G., et al. 2000, AJ, 120, 1579
Zentner, A. R., & Bullock, J. S. 2002, Phys. Rev. D, 043003-1
Zwaan, M. 2001, MNRAS, 325, 1142
Zwaan, M. A., & Briggs, F. H. 2000, ApJ, 530, L61
Zwaan, M., et al. 2005, MNRAS, 365, 1467